Phenomenological Modeling of Sheet Moulding Compound Composites Under Quasi-Static Three-Point Bending

by

Jonathan Chun-Yiu Tham

A thesis
presented to the University of Waterloo
in fulfillment of the
thesis requirement for the degree of
Master of Applied Science
in
Mechanical and Mechatronics Engineering

Waterloo, Ontario, Canada, 2018

I hereby declare this thesis consists of material all of which I authored or co-authored: see Statement of Contributions included in the thesis. This is a true copy of the thesis, including any required final revisions, as accepted by my examiners.

I understand that my thesis may be made electronically available to the public.

Statement of Contributions

I would like to acknowledge the following parties for their contributions to the work in this thesis:

Dr. Kaan Inal supervised this MASc thesis.

Dr. Julie Lévesque performed and provided the experimental results for the tensile and compressive tests.

General Motors provided the experimental results for the in-plane shear tests.

Anna Trauth performed and provided the experimental results for the three-point bend test.

Dr. Christopher Kohar provided code for the implementation of the yield function.

Trevor Sabiston assisted in the editing of this work.

The balance of this work is my own.

Abstract

A phenomenological model is implemented to model the behaviour of a glass fiber reinforced sheet moulding composite material. Previous characterization of SMC composites, which included the tensile, compressive, in-plane shear and three-point flexure test, found that the material exhibits tension-compression asymmetry and in-plane anisotropy. Based on the experimental results, a model, which incorporates an anisotropic and asymmetric yield function, is implemented in LS-DYNA as a user-defined material model. The model is calibrated to the experimental tension, compression and in-plane shear test results and is validated using the experimental three-point flexure test results. The model is able to capture the flexure stress-strain response within 8% of experimental results. Parametric studies are conducted to determine the sensitivity of the flexure test simulation results to various modeling and material parameters.

Acknowledgements

I would like to thank Dr. Kaan Inal for his mentorship and guidance as my supervisor, which has helped me become a better researcher. I would also like to thank Trevor Sabiston for being a great mentor, providing guidance and expertise in composite materials. I would also like to acknowledge Dr. Julie Lévesque, Anna Trauth and General Motors for performing the experiments required, which has been essential in calibrating the model in this work. I would also acknowledge Dr. Christopher Kohar for providing code for the yield function, which has helped to accelerate this work. I would like to thank my colleagues at the CMRG group for their support. I would like to thank my family and friends for their support and motivation over the years. Finally, I would like to thank the Natural Sciences and Engineering Research Council of Canada (NSERC) and General Motors for their financial support.

Table of Contents

List of Tables

List of Figures

Chapter 1

Introduction

As fuel economy and safety regulations in the automotive industry [5] become stricter, vehicle manufacturers are becoming more focused on weight reduction and improving crashworthiness. A reduction of vehicle mass by 10% results in a 6.8% fuel economy improvement [6, 7]. Sources of improvement in weight reduction and crashworthiness include material selection and component design optimization [8]. As a result, interest in composite materials for mass production vehicle components is increasing significantly. In the past, composites were mostly used in low production volume vehicles as composite components were manufactured through low volume production methods, such as hand lay-ups, which were slow and expensive [9]. High production volume manufacturing methods, such as compression moulding, decrease the material and manufacturing costs and makes composite materials, such as Sheet Moulding Compounds (SMC), significantly more viable for mass-production vehicles [10]. Due to the different manufacturing process used, SMC composites have misaligned discontinuous fibres, while composite lay-ups which have continuous and aligned fibres. The type of fibres used influences the performance and cost of the composite, continuous fibres have higher performance and higher cost than discontinuous fibres [11]. Due to the lower performance of discontinuous fibre composites compared to continuous fibre composites, SMC composites are more suitable for secondary vehicle structures, such as exterior body panels [9], instead of primary load-bearing structures.

The benefit of using composite materials is the ability to optimize the material for the application. Depending on the type of reinforcement and matrix material, composites can have a higher strength and stiffness to weight ratio than metals [12, 11]. By having a higher specific strength and stiffness, a composite component with a lower mass is able to absorb the same amount of energy during an impact. This makes composite material good for reducing the mass and improving crashworthiness of vehicles.

In addition to optimizing composite material properties through different material combinations, composites such as fibre-reinforced polymers can have significant anisotropy, which can be a benefit when designing parts using composite materials. The fibre orientations can be tailored to the load cases experienced by the component, optimizing the amount of material required [13, 14, 11].

An important aspect of designing vehicle components made of composite materials is verifying the performance of the components. Vehicle manufacturers use Finite Element Analysis (FEA) to reduce the development cost and time, as designs can be verified in simulations before a promising design is produced and physically tested. There is a need for development in FEA techniques to grow the use of composite materials in vehicle component design. In order to be able to use FEA for modeling the structural behaviour of composite components accurately, a material model which is capable of capturing the fundamental behaviour of composite materials is required. The model not only has to be accurate, but also fast, in order to reduce the development time of composite components [15].

1.1 Research Objective

In order to be able to accurately model SMC composite vehicle components subjected to complex load cases, the material model must first be able to capture the fundamental behaviour of the material in simpler load cases, such as standardized material tests. Therefore, the objective of this work is to be able to model the behaviour of SMC composite materials accurately using a phenomenological material model. This model aims to be able to capture the complex behaviour of the material in various load cases such as tension, compression, in-plane shear and three-point bending. By capturing the behaviour in these load cases, the model will be able to capture the behaviour of the material in more complex load cases experienced by vehicle components, such as the exterior body panels which can be made from SMC composites. The model is implemented as a user-defined material model in the commercial finite element software, LS-DYNA and is calibrated using experimental data for the tension, compression and in-plane shear tests. The calibrated model is validated by using it to predict the bending behaviour of the composite. Parametric studies are performed on the through-thickness variation in material properties, friction in the testing fixture, the assumptions made for the out-of-plane properties and the presence of tension-compression asymmetry, to determine their effect on the prediction of flexure response.

1.2 Thesis Outline

Following this introduction, Chapter 2 will cover the background information regarding composite materials, SMC materials and existing work on characterizing and modeling composite materials.

In Chapter 3 the behaviour of the SMC material studied in this thesis is determined through the analysis of the results of previous experimental testing performed by Dr. Julie Lévesque, Anna Trauth and General Motors. This includes some details of the specimen and test setup and the results of the testing. The tests which were conducted are the tensile, compressive, in-plane shear and three-point bend test.

Using the information from the results of the experimental testing, Chapter 4 describes the constitutive modeling required to capture the behaviour of the SMC material. This section also covers the implementation of the constitutive model into a LS-DYNA user-defined material model to allow it to be used in a finite element simulation.

The implemented model is calibrated to experimental data in Chapter 5. Using the calibrated model, the flexure test is simulated and compared to experimental data to validate the model.

Chapter 6 describes the parametric studies performed to study the effects of various modeling and material parameters on the flexure behaviour.

Finally, Chapters 7 and 8, summarise the results of this work, improvements which can be made to the model and future extensions to this work.

Chapter 2

Background

Composites are materials consisting of two or more distinct constituents [16]. A composite material combines the strengths of its constituents, with the effects of each phase being determined by its volume fraction [16]. In a two-phase composite, the reinforcement phase is used to provide stiffness and strength to the composite, while the matrix phase holds the reinforcements together to form the composite [16]. A composite can have particle or fibre reinforcements [16]. A widely used form of composites in the automotive industry is fibre reinforced polymers, which are typically reinforced by glass or carbon fibres.

Fibre reinforced polymers (FRP) can have various fibre reinforcement structures. Depending on fibre length, there are continuous and discontinuous FRP's [17]. Discontinuous FRP can also be broken down into aligned FRP and randomly oriented FRP [17]. The reinforcement structure significantly affects the material properties and anisotropy of the composite. The reinforcement structure is usually determined by the manufacturing method or process of the composite.

As described, the addition of fibres to the matrix material makes the behaviour of the composite more complex than the individual phases, which increases the difficulty of accurately modeling the composite behaviour. Various micromechanical factors which include the orientation, volume fraction and distribution of the fibres in the matrix material have a significant effect on the material response. The manufacturing process of the composite determines its fibre structure, and therefore affects the material behaviour. The presence of filler material or material defects, such as voids, can also affect the composite material behaviour [16].

Two types of polymers, thermosets and thermoplastics, are used in FRP. Thermosets start as semi-solids that can melt and flow during the curing process, as it is cured covalent

bond cross-links form between the polymer chains [11]. Thermoplastics consist of polymer chains held together with secondary bonds and are fully reacted before processing [11]. Unlike thermosets, thermoplastics do not form cross-links when cured [11]. The lack of cross-links allows thermoplastics to be reprocessed unlike thermosets [11].

2.1 Manufacturing Methods

The manufacturing and processing methods vary for the type of fibre reinforcement and matrix material used in the FRP composite. Thermoplastics require a significantly higher curing temperature than thermosets [11]. However, thermoplastics can be cured more quickly, as cross-links do not need to be formed through chemical reactions [11].

There are many variations of composite manufacturing methods, three of the main methods are lay-ups, compression moulding and resin transfer moulding. The manufacturing methods differ in cost, cycle time and the type of composite which can be produced, and therefore are suitable for different applications.

2.1.1 Lay-ups

The use of lay-ups is the traditional method of manufacturing composites. There are multiple variations of the lay-up method. In one variation, layers of pre-impregnated fibre or woven fabric are laid on a mould and cured to form a laminate [11]. Another variation uses a wet lay-up method where resin material is applied after each layer of dry reinforcement is laid [11]. Depending on the type of matrix and fibre and the desired end product, there are multiple curing methods including in and out of autoclave [11]. The orientation of the fibres in each lamina can be used to tailor the properties of the composite [14, 11]. Due to the continuous and aligned fibres, this type of composite is strong and stiff [11]. However, this manufacturing process can be slow [18] and expensive [10].

2.1.2 Compression Moulding

In compression moulded composites, the uncured material is formed in mould using a moulding tool and cured under pressure and heat. As the material is heated and compressed, the material flows and fills the mould to form the final component [11]. Most compression moulding processes use a form of moulding compound which is a charge or

blank consisting of a mixture of fibre reinforcement and matrix material [11]. In the case of SMC composites, this material is in the form of sheets containing discontinuous fibre reinforcements. The manufacturing method for the charges and the moulding process can affect the fibre orientation of the final component and in turn affect the material properties [19, 20, 21]. The use of SMC and compression moulding can significantly reduce the cost of composite components [10].

2.1.3 Resin Transfer Moulding

Another manufacturing method capable of reducing the cost of composites is resin transfer moulding (RTM) [10]. It involves holding fibre reinforcement material in a closed mould, followed by pumping of resin material into the mould where it surrounds and coats the fibre reinforcements [22]. The composite is cured in the mould and reinforced by the fibre material [22]. Similar to compression moulding, this manufacturing process results in a significantly cheaper overall cost than hand lay-ups [10].

2.1.4 Comparison of Manufacturing Methods

Based on a cost estimate in literature for a carbon fibre reinforced epoxy component, a compression moulded SMC component is the most cost effective, while an autoclave cured lay-up is the least cost effective for the same mechanical performance [10]. Compression moulding is approximately 70% cheaper than autoclave cured composites and 35% cheaper than resin transfer moulding [10]. Due to the cost effectiveness of SMC composites, vehicle manufacturers are becoming more interested in designing and manufacturing vehicle components from SMC composites.

In addition to being more cost effective, compression moulding is capable of producing parts at a higher rate compared to using prepreg lay-ups [23]. The cycle time of compression moulded and RTM composites is a few minutes, while the cycle time for prepreg lay-ups is more than 5 hours [18].

The type of manufacturing method used is also determined by the geometry of the part. Large components or components which require some type of core material can be manufactured using some types of lay-up and RTM processes [11].

2.1.5 Manufacturing of SMC Composites

The sheet moulding compound for use in a compression moulded composite is manufactured by the addition of chopped fibres onto a layer of resin paste consisting of thermosetting polymer and filler material which is carried along by a carrier film [11]. After the fibres are added, a second layer of resin paste is added on top to sandwich to the fibres [11]. The stack of material is then compacted by rollers and stored as a roll of SMC material [11]. An illustration of the SMC production process can be found in Manufacturing Processes for Advanced Composites by F.C. Campbell [11].

SMC charges are cut to size from the roll of material for the compression moulding process. One or more charges are placed in a mould, before the mould is closed [11]. The material is heated and compressed in the mould using a press [11]. As it is compressed, the material flows to fill the mould [11]. The material is cured in the mould under pressure and heat [11]. After the material has been cured the mould is opened and the finished component is released from the mould. The moulding process of a SMC composite is shown in Figure 2.1.

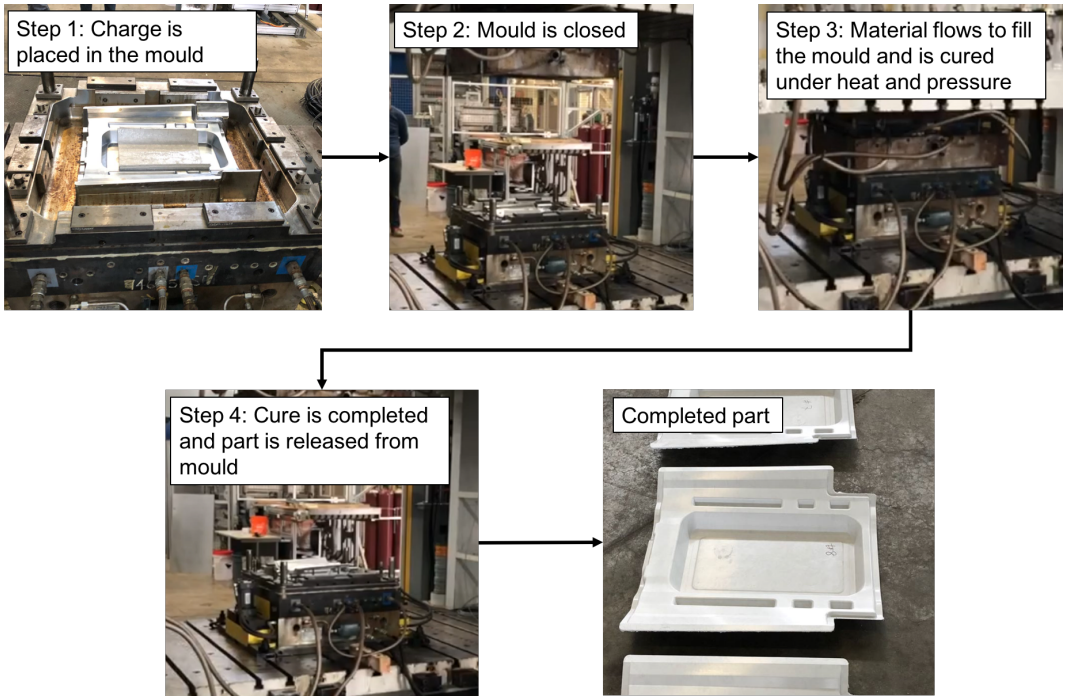

Figure 2.1: Moulding process of a SMC composite

2.2 Behaviour of SMC Materials

Due to the low volume fraction of fibre material in SMC composites the elasto-plastic behaviour of the thermoset matrix phase is more dominant than the linear elastic fibres, resulting in a non-linear composite stress-strain response. In addition to the complex behaviour resulting from the introduction of fibre into matrix material in a composite, SMC composites have misaligned discontinuous fibres which increases the complexity of the material behaviour. SMC materials also exhibit complex phenomenon such as anisotropy, due to manufacturing process [21, 24], or tension-compression asymmetry, due to geometric effects, damage evolution and matrix behaviour [25, 26, 27].

2.2.1 Process-Induced Anisotropy

Due to the manufacturing process of SMC composites, the fibres are not completely randomly oriented. Due to the flow of material during the manufacturing of the charge and during the moulding process, the fibres can align in certain directions [19, 20]. This phenomenon results in anisotropy in the final product.

Through experiments with various degrees of mould coverage, Feld et al. [21] studied the degree of process-induced anisotropy. It was found that both the moulding process and SMC charge manufacturing process introduced anisotropy to the material [21]. This is determined from the existence of anisotropy in the moulded material even with almost full mould coverage [21]. The decrease in mould coverage also increased the elastic stiffness in the strain or flow direction while decreasing it in the transverse direction [21].

Oldenbo et al. studied the effects of moulding process-induced anisotropy by performing an analysis to determine the effect of process-induced fibre orientation on the global stiffness of a vehicle hood [24]. The model calculates the stiffness tensor using the fibre orientation tensor and micromechanics model with an aligned ellipsoidal inclusion [24]. It is shown that charge placement can reduce the degree of anisotropy of the final component [24].

2.2.2 Tension-Compression Asymmetry

In addition, to orientation dependent properties, a material can also have different properties depending on whether the load is tensile or compressive. This phenomenon is observed in most composites in literature. It is a combined effect of the molecular and crystalline structure of the polymer matrix, the buckling of fibres in compression and the difference in damage evolution in tension and compression [25, 26, 27].

From experimental testing on several thermoplastic polymers in tension and compression, Donato et al. observed tension-compression asymmetry in yielding of the polymer materials, where the yield strength under a compressive load was greater than a tensile load [25]. Tension-compression asymmetry in polymers is also observed by several others in literature [28, 29, 30].

In literature, the tension-compression asymmetry was also studied in fibre reinforced composite materials. Hartl et al. [26, 27] studied the anisotropy and tension-compression asymmetry in fibre reinforced polypropylene. Hartl et al. observed that the anisotropy is affected by the tension-compression anisotropy, a higher degree of anisotropy was observed in tension [26]. The tension-compression anisotropy is also observed to be affected by fibre orientation and length [26]. Tension-compression asymmetry in the fibre direction decreases as fibre length increases, while the opposite happens in the in-plane transverse direction [26].

In addition to tension-compression asymmetry in yielding, asymmetry in the elastic stiffness of polymers is also observed in literature [31]. Elleuch et al. performed monotonic tensile and compressive characterization of high-density polyethylene at various strain rates [31]. In addition to observing the viscoelastic effect on the tangent elastic modulus, the material also appeared to be stiffer in compression than tension at all three strain rates tested [31].

2.3 Micromechanics and Multi-Scale Modeling

Modeling of composite materials can be performed at various length scales, depending on the resolution of the results or computational efficiency required. Micromechanics is used to model the behaviour at a microscopic level accurately. The fibre and matrix phases are modeled as separate components. In unidirectional composites with a periodic fibre structure, the composite properties can be predicted by modeling a representative volume element (RVE) [32, 33, 34]. This approach works well for unidirectional composites with easily identifiable RVE, but not for composites with randomly oriented and discontinuous fibres, such as SMC composites. In addition, modeling the micromechanical structure of the entire component using this approach is not feasible for FEA of large components as capturing the fibre structure accurately, would require a large number of extremely small elements in the finite element mesh. Performing a FEA simulation on such a large model would require a large amount of computational resources. In addition, the properties of the constituents, which are required for a micromechanics approach, are not always readily

available. The in-situ matrix properties can also differ from the neat matrix properties [34].

Micromechanics-based multi-scale approaches use homogenization methods to determine the average properties of the composite, without having to model the individual constituents when creating the finite element model. Some of the more commonly used homogenization methods include the Voigt, Reuss and Mori-Tanaka homogenization schemes. The Voigt homogenization scheme assumes a constant mean strain, while the Reuss homogenization scheme assumes a constant mean stress, they represent the upper and lower bounds of the solution [35]. The Mori-Tanaka homogenization scheme assumes that the mean stress in the matrix of the composite is constant [36]. These homogenization schemes are suitable for composites with continuous aligned fibre structures. Extensions have been made to these approaches for misaligned fibre composites [35, 37].

The multi-scale micromechanics approaches taken by Lielens et al. and Doghri et al. to model misaligned fibre composites use a method which represents the composite using a pseudo-grain model, where each grain represents a group of aligned fibres [35, 37]. Homogenization is performed on each grain followed by a second homogenization is performed to obtain a single homogenized material response [35, 37].

In a micromechanics approach, it is also important to account for the interaction between the fibre and matrix. In literature, some researchers have modeled the interface, the surface where the fibre meets the matrix phase, with cohesive zone models which allow for the separation between the fibre and matrix at the interface [38, 39]. Others have used an interphase, a third phase surrounding the inclusion, to capture the interaction between the fibre and matrix [40, 41, 42]. This can be accounted for in a multi-scale modeling approach using a homogenization method developed by Benveniste et al. [43]. Benveniste et al. extended the Mori-Tanaka approach to be applied to coated inclusions which are considered to have three phases [43]. This approach is applied to account for the interphase region in multi-scale approaches, where the interphase region is the phase coating the fibres [40, 41, 42].

Sabiston et al. introduced a homogenization model capable of maintaining stress and strain compatibility between the matrix and fibre using a functionally graded interphase zone [44, 45]. The model was used to predict the elasto-visco-plastic behaviour of long fibre composites [44, 45]. The predicted stress in the interphase zone can be useful when modeling failure.

Micromechanics based approaches also have the potential to predict the local stress and strain variation. Carmen et al. uses a micromechanics model to predict the overall composite stiffness and local stress and strain variations of a short-fibre composite [46].

This is potentially beneficial for the prediction of fracture or damage in the composite.

Although micromechanics based approaches offer increased modeling accuracy and insight into local material behaviour, the properties of each constituent, information on the fibre orientation, and a method to account for fibre orientation and interaction between the constituents is required [47]. Finally, these approaches are typically more computationally expensive compared to macro-scale phenomenological models [48, 47].

2.4 Phenomenological Modeling

A phenomenological model describes experimentally observed phenomenon without the use of micromechanical theory. A phenomenological model is calibrated to a set of data obtained from experiments. In a macro-scale phenomenological model, the composite is modeled as a single phase. The benefits of such a model include faster performance due to less computations being required, which in return requires less computation resources and time than multi-scale or micromechanics models [48]. In addition, calibration of such a model for composite materials is simplified since the properties of each individual phase is not required. The disadvantage of using a phenomenological model is the need to re-calibrate the model if the fibre structure is changed, which includes changes to the fibre volume fraction or fibre orientation distribution.

It is important for the phenomenological model to capture both the elastic and plastic behaviour of the composite introduced by the matrix phase due to low fibre volume fraction in SMC composites [17].

In order to use a phenomenological approach to model the stress-strain response of a composite material, yield functions capable of capturing the complex non-linear plastic behaviour, such as tension-compression asymmetry or in-plane anisotropy, caused by fibre orientation distribution [21, 24], are required.

2.4.1 Elasticity

In solid mechanics, elasticity describes the fully reversible portion of the stress-strain relationship of a solid material [47]. It is described by the generalized Hooke's law [49], shown in equation 2.1, which relates stress, σ, to strain, ε, with an elastic stiffness tensor. The coefficients, c, in the stiffness tensor depend on the material behaviour.

$$\begin{bmatrix} \sigma_{11} \\ \sigma_{22} \\ \sigma_{33} \\ \sigma_{12} \\ \sigma_{23} \\ \sigma_{31} \end{bmatrix} = \begin{bmatrix} c_{1111} & c_{1122} & c_{1133} & c_{1112} & c_{1123} & c_{1131} \\ c_{2211} & c_{2222} & c_{2233} & c_{2212} & c_{2223} & c_{2231} \\ c_{3311} & c_{3322} & c_{3333} & c_{3312} & c_{3323} & c_{3331} \\ c_{1211} & c_{1222} & c_{1233} & c_{1212} & c_{1223} & c_{1231} \\ c_{2311} & c_{2322} & c_{2333} & c_{2312} & c_{2323} & c_{2331} \\ c_{3111} & c_{3122} & c_{3133} & c_{3112} & c_{3123} & c_{3131} \end{bmatrix} \begin{bmatrix} \varepsilon_{11} \\ \varepsilon_{22} \\ \varepsilon_{33} \\ \varepsilon_{12} \\ \varepsilon_{23} \\ \varepsilon_{31} \end{bmatrix} \tag{2.1}$$

The elastic response of a material can depend on the material orientation. An isotropic elastic material is a material which elastic properties do not depend on the orientation of the material. On the other hand, anisotropy describes materials where the properties depend on the direction or orientation. Anisotropy can be the result of factors such as the microstructure orientation in metals or due to the alignment of fibres in a composite material. Taking anisotropy into account is important when designing components from a material known to be anisotropic, it will allow the optimal orientation of the material for the loads the component is designed to handle [13, 14, 11]. Anisotropy can be simplified to several cases, such as orthotropy or transverse isotropy, for modeling purposes.

Orthotropy is a special case of anisotropy where the material properties are different in the three mutually orthogonal directions. Orthotropy in elasticity can be modeled through the use of an orthotropic elastic stiffness tensor shown in equations 2.2 and 2.3, where E are the elastic moduli, G are the shear moduli and v are the Poisson's ratios [50].

$$\mathbb{L}_{el} = \begin{bmatrix} \frac{1-v_{23}v_{32}}{E_2E_3\Delta} & \frac{v_{21}+v_{31}v_{23}}{E_2E_3\Delta} & \frac{v_{31}+v_{21}v_{32}}{E_2E_3\Delta} & 0 & 0 & 0 \\ \frac{v_{12}+v_{13}v_{32}}{E_3E_1\Delta} & \frac{1-v_{31}v_{13}}{E_3E_1\Delta} & \frac{v_{32}+v_{31}v_{12}}{E_3E_1\Delta} & 0 & 0 & 0 \\ \frac{v_{13}+v_{12}v_{23}}{E_1E_2\Delta} & \frac{v_{23}+v_{13}v_{21}}{E_1E_2\Delta} & \frac{1-v_{12}v_{21}}{E_1E_2\Delta} & 0 & 0 & 0 \\ 0 & 0 & 0 & 2G_{12} & 0 & 0 \\ 0 & 0 & 0 & 0 & 2G_{23} & 0 \\ 0 & 0 & 0 & 0 & 0 & 2G_{31} \end{bmatrix} \tag{2.2}$$

$$\Delta = \frac{1 - v_{12}v_{21} - v_{23}v_{32} - v_{31}v_{13} - 2v_{12}v_{23}v_{31}}{E_1E_2E_3} \tag{2.3}$$

Transverse isotropy is another special case of anisotropy where there exists a plane which exhibits an isotropic response, while the normal direction to the plane exhibits a different response. A sheet material with fibres orientated in each direction equally is transversely isotropic with respect to the normal direction of the sheet, while a unidirectional composite is transversely isotropic about the fibre direction.

2.4.2 Yield Functions

In a phenomenological plasticity approach, the yield function in combination with the hardening rule determines how the material yields for various stress states. The yield function describes the combination of stress components that would result in yielding or plastic deformation of the material, while the hardening rule defines how the yield surface expands upon yielding [51]. Yield functions exist for various material phenomenon, including anisotropy and tension-compression asymmetry.

Von Mises Yield Function

One of the most commonly used yield functions is the von Mises yield function. It is an isotropic yield function given by equation 2.4, where σ_i are the principal stresses. Yielding occurs when the effective stress, σ_{vM}, exceeds the yield stress [52, 53, 25].

$$\sigma_{vM} = \frac{1}{\sqrt{2}} \cdot \sqrt{(\sigma_1 - \sigma_2)^2 + (\sigma_2 - \sigma_3)^2 + (\sigma_3 - \sigma_1)^2} \tag{2.4}$$

Due to the orientation of fibres in a composite, which can result in significant anisotropy, the use of an isotropic yield function will not be sufficient to capture its yielding behaviour.

Hill-48 Yield Function

Hill developed an orthotropic yield criterion, defined by equation 2.5, where the yielding in the principal anisotropic directions, which includes three normal and three shear directions, are captured using six parameters, F, G, H, L, M and N [54]. The anisotropic parameters are calculated with equations 2.6 to 2.11 [54]. X, Y and Z are the tensile yield stresses, while R, S and T are the yield stresses in shear with respect to the principal anisotropic directions [54].

$$\sigma_{Hill-48} = F(\sigma_y - \sigma_z)^2 + G(\sigma_z - \sigma_x)^2 + H(\sigma_x - \sigma_y)^2 + 2L\tau_{yz}^2 + 2M\tau_{zx}^2 + N\tau_{xy}^2 \tag{2.5}$$

$$2F = \frac{1}{Y^2} + \frac{1}{Z^2} - \frac{1}{X^2} \tag{2.6}$$

$$2G = \frac{1}{Z^2} + \frac{1}{X^2} - \frac{1}{Y^2} \tag{2.7}$$

$$2H = \frac{1}{X^2} + \frac{1}{Y^2} - \frac{1}{Z^2} \tag{2.8}$$

$$2L = \frac{1}{R^2} \tag{2.9}$$

$$2M = \frac{1}{S^2} \tag{2.10}$$

$$2N = \frac{1}{T^2} \tag{2.11}$$

Although the Hill-48 yield function is able to capture anisotropy in the normal directions and shear, it is limited in its ability to capture both yield stress variation and the Lankford coefficients, which describe the plastic strain ratio, at the same time [55]. In addition, it is also unable to capture the tension-compression asymmetry observed in SMC composites.

Barlat-89 Yield Function

Barlat et al. developed a non-quadratic yield criterion for orthotropic materials under plane stress, which provides improved predictions in biaxial stress states [56]. This yield criterion was later extended by Barlat et al. for use in three-dimensional stress states [57].

Similar to the Hill-48, this yield function is capable of capturing anisotropy, but limited in its ability to capture tension-compression asymmetry, and both the yield stress variation and Lankford coefficients at the same time [55]. Therefore, this model is not suitable for the SMC composite studied.

Barlat YLD2000 Yield Function

Barlat et al. developed a general non-quadratic anisotropic yield function, YLD2000, where anisotropy is determined by linear transformations on the stress tensor [58]. The transformation matrix contains the coefficients controlling anisotropy [58].

Unlike the Hill-48 and Barlat-89 yield functions, this yield function is able to capture both the yield stress variation and the Lankford coefficients. However, similar to the other two yield functions, it does not capture the tension-compression asymmetry which needs to be considered in a SMC composite.

Pressure Sensitive Yield Function

Due to the observed tension-compression asymmetry in polymers and polymer composites, a yield function capable of capturing this phenomenon is required. Polymers exhibit tension-compression asymmetry in yielding due to the arrangement of the polymer chains and the deformation mechanisms, such as shear banding or crazing, which are influenced by the hydrostatic pressure [25, 59].

Pressure sensitive yield criteria fall into this category. Pressure sensitive yield criteria have a dependence on the hydrostatic pressure. The hydrostatic pressure can be expressed in terms of the first stress invariant, I_1, as shown in equation 2.12. The first stress invariant is calculated using equation 2.13, where σ_i are the principle stresses [25].

$$\sigma_{hyd} = \frac{I_1}{3} \tag{2.12}$$

$$I_1 = \sigma_1 + \sigma_2 + \sigma_3 \tag{2.13}$$

In addition to experimental testing to characterize the tension-compression asymmetry in several polymers, Donato et al. evaluates the effectiveness of two pressure sensitive yield criteria in capturing the observed tension-compression asymmetry [25]. The two yield criteria they studied are the conically and parabolically modified von Mises yield criteria [25]. As the names suggest, they are based on the von Mises yield criterion. The conically modified yield criterion contains a linear hydrostatic dependent term, while the parabolic modified yield criterion contains a quadratic hydrostatic dependent term [25].

Although the yield functions studied by Donato et al. are able to capture the tension-compression asymmetry of a material, they are based on the von Mises yield criterion, and therefore they are unable to capture the anisotropy in yielding. The required yield function has to capture both tension-compression asymmetry and anisotropy in yielding, such as the yield function developed by Cazacu et al. [60].

Cazacu-Plunkett-Barlat Anisotropic Yield Function

Another yield function capable of capturing tension-compression asymmetry is the yield criterion (CPB) developed by Cazacu et al. [60]. The yield criterion is able to capture anisotropy in addition to the tension-compression asymmetry. Unlike the conically and parabolically modified von Mises yield criteria, this yield criterion is pressure independent. The CPB yield criterion is able to capture the tension-compression asymmetry through the use of the k parameter shown in equation 2.14 [60]. The degree of asymmetry can also be controlled through the a exponent [60]. This yield criterion also captures the in-plane orthotropy through a linear transformation of the deviatoric stress tensor, $\mathbf{S}$, with the transformation tensor, $\mathbb{C}$, to obtain Σ, shown in equation 2.15 [60]. The transformation tensor is defined in equation 2.16. C_{ij}, where $i = 1:3$ and $j = 1:3$, control the orthotropy in normal directions, while C_{ii} where $i = 4:6$ control the orthotropy in shear [60]. Σ_i are the principal values of the transformed stress tensor. Cazacu et al. applied this yield criterion to modeling hexagonal closed packed (HCP) metals such as magnesium and titanium alloys [60].

$$(|\Sigma_1| - k \cdot \Sigma_1)^a + (|\Sigma_2| - k \cdot \Sigma_2)^a + (|\Sigma_3| - k \cdot \Sigma_3)^a = F^a \tag{2.14}$$

$$\Sigma = \mathbb{C} : \mathbf{S} \tag{2.15}$$

$$\mathbb{C} = \begin{bmatrix} C_{11} & C_{12} & C_{13} & 0 & 0 & 0 \\ C_{12} & C_{22} & C_{23} & 0 & 0 & 0 \\ C_{13} & C_{23} & C_{33} & 0 & 0 & 0 \\ 0 & 0 & 0 & C_{44} & 0 & 0 \\ 0 & 0 & 0 & 0 & C_{55} & 0 \\ 0 & 0 & 0 & 0 & 0 & C_{66} \end{bmatrix} \tag{2.16}$$

The yield function developed by Cazacu et al. is able to capture the tension-compression asymmetry and anisotropy in yielding of a material, therefore it is capable of modeling the SMC composite, which is observed to exhibit these properties in literature and experiments. In addition, it can be used to capture both the variation in yield stresses and the Lankford coefficients. Therefore, this yield function is used in combination with a hardening model to capture the behaviour of the SMC composite in this thesis.

2.4.3 Hardening Model

In order to describe the hardening of the material in a phenomenological plasticity approach, a hardening rule (curve) is used to relate the effective plastic strain to the flow stress.

One of the simpler and more widely used hardening rules is the power law hardening rule. It relates the flow stress to the effective plastic strain of the material with a power law function [61, 62]. One form of the power law, Ludwik's equation, is shown in equation 2.17 [62]. $\bar{\sigma}$ is the flow stress, σ_y is the yield stress, $\bar{\varepsilon}_p$ is the effective plastic strain, K is the strength coefficient and n is the strain hardening exponent [62].

$$\bar{\sigma} = \sigma_y + K(\bar{\varepsilon}_p)^n \tag{2.17}$$

Some hardening rules are able to capture temperature and strain rate effects for materials which exhibit sensitivity to such parameters. Extensions have been made to power law hardening rules to capture temperature and strain rate effects in models such as the Johnson-Cook model [63], shown in equation 2.18. ε, $\dot{\varepsilon}$ and T are the strain, strain rate and temperature respectively. The first part of the expression is a power law expression describing strain hardening at the reference strain rate and at room temperature, where A is the initial yield stress, B is the strength coefficient and n is the strain hardening exponent [63]. The second part of the expression is a logarithmic term which determines the strain rate sensitivity of the yielding of the material, where $\dot{\varepsilon}_0$ is the reference strain rate and C controls the degree of sensitivity to strain rate [63]. The third part of the expression determines the temperature sensitivity of the yielding of the material, where T_{room} is the room temperature, T_{melt} is the melting point temperature and m is the exponent that determines the degree of sensitivity to temperature [63].

$$\bar{\sigma} = [A + B\varepsilon^n]\left[1 + Cln\left(\frac{\dot{\varepsilon}}{\dot{\varepsilon}_0}\right)\right]\left[1 - \left(\frac{T - T_{room}}{T_{melt} - T_{room}}\right)^m\right] \tag{2.18}$$

With the experimental results available for the material studied in this thesis, the power law hardening rule is able to capture the non-linear plastic behaviour, and therefore is used in the material model implemented. In order to be able to implement a strain rate or temperature sensitivity model, additional material testing data at various temperature and strain rates is recommended.

2.4.4 Commercially Available (LS-DYNA) Composite Material Models

One of the leading commercial finite element software used for automotive structural and crashworthiness analysis is LS-DYNA. Several composite material models designed to model fibre reinforced composites are available in the commercial finite element software, LS-DYNA [61, 64].

The first model which can be used to model composites is a general orthotropic elastic model (MAT_002) [64, 61]. Due to its fibre orientation, a composite can exhibit orthotropy. This is useful for composites which exhibit a linear elastic stress-strain response. LS-DYNA also has composite specific models which incorporate some type of brittle failure criteria. These models include the composite damage material model (MAT_022) and the enhanced composite damage material model (MAT_054 and MAT_055) [64, 61]. Majority of the material models are more applicable to unidirectional composite or laminates containing unidirectional layers.

The composite damage material model [64, 61] allows for the implementation of brittle failure through the use of the Chang and Chang failure criteria [65] for fibre and matrix failure modes. There are two variations of the enhanced composite damage model. Both material models use the Chang and Chang criterion for compressive matrix failure [64, 61]. The first variation (MAT_054) also uses the Chang and Chang criterion for fibre failure and tensile matrix failure, while the second variation (MAT_055) uses the Tsai-Wu criteria for those failure modes [64, 61]. These three models allow for progressive damage, by reducing the stiffness of each layer that is found to fail based on the failure criteria and upon failure of all layers through the thickness, the element is removed [64, 61]. The failure criteria used in these models are limited to unidirectional lamina.

The laminate composite fabric material model (MAT_058) is a composite material model with damage for unidirectional, laminated and fabric composites [64, 61]. The damage model, based on the model developed by Matzenmiller et al. [66, 67], reduces the elastic stiffness as the damage accumulates. It also allows for a minimum stress limit, which limits the drop in stress after the failure stress is reached and only removes the element when the maximum effective strain is exceeded [64, 61]. This allows for a non-linear stress-strain behaviour to be modeled. In addition, depending on the type of failure surface used, it can also be applied to laminated fabric composites. The composite failure material model (MAT_059) is another composite material model that can model a non-linear stress-strain behaviour [64, 61] by using the material strength values in a yield function to form a failure surface [68].

The composite lay-up material model (MAT_116) uses standard composite lay-up theory, which precalculates the extensional, bending and coupling stiffness which relate the curvatures and strains to the forces and moments [64, 61]. The composite matrix material model (MAT_117) and the composite direct material model (MAT_118) are similar to the composite lay-up material model, however, the extensional, bending and coupling stiffness are calculated and input to the material model by the user [64].

The limitations of the existing composite models are that they are typically used for unidirectional or laminated composites. In addition, many of them are designed to be used with shell elements where the thickness of the geometry is significantly lower than the other dimensions, however this is not always the case. In addition, the available damage models' ability to capture non-linear stress-strain behaviour is a function of the failure strength and failure strain and does not account for the plasticity caused by the polymer matrix material.

There have been existing attempts at modeling the behaviour of composite components using these models, however, most of these simulations are performed on laminated composites which have a brittle failure mode, unlike SMC materials which have a lower fibre volume fraction and hence a more matrix dominated behaviour.

An example of a component level simulation of a composite using commercially available material models is by Huang et al. [69], they performed simulations of axial crushing of carbon fibre reinforced laminated composite tubes and compared the predicted response to the quasi-static experimental response. The LS-DYNA enhanced damage composite model (MAT_054) for thin shell elements which uses the Chang and Chang failure criteria was used to model the composite material. In order to account for the delamination of the composite, the model was made up of two layers of elements joined using a tiebreak contact definition, which allows for the breaking of contact when a criterion involving the normal and shear stress at the contact is satisfied [69]. The model was able to capture the general trend of experimental load-displacement curves and is able to capture the failure mode of the composite tube [69]. The enhanced damage composite model was also used by El-Hage et al. to model the axial crushing of glass-fibre reinforced epoxy in aluminum-composite hybrid tubes and the effect of friction and adhesion between the aluminum tube and composite wrap. [70]. The interface between the aluminum tube and composite wrap is modeled by a tiebreak contact definition [70]. The predicted overall crush response of the two types of tubes tested, including the folding initiation forces and mean crushing forces, was very close to the experimentally measured crush response [70].

Xiao et al. also simulated the axial crushing of carbon fibre reinforced tubes manufactured using resin transfer moulding [67]. They used the LS-DYNA laminated composite

fabric material model (MAT_058) which uses a damage model to reduce the stiffness of the material as damage accumulates [67]. The simulation was able to predict the peak force of the axial crush fairly well, however, it underpredicted the average crush force [67]. From the comparison of experimental testing and simulation results of the composite material coupon specimen loaded first in compression then tension, it was found that the model was significantly underpredicting the tensile stiffness of the damaged specimen [67]. It was concluded that this was likely to be the cause of the underprediction of average crush force [67].

Mamalis et al. [71] also modeled the behaviour of composite tubes using the available material models in LS-DYNA. From preliminary investigation, they found that the second variation of the enhanced composite damage model (MAT_055) best captured the response of the axial crushing of the composite tube compared to the first variation of the enhanced composite damage model (MAT_054) and the laminated composite fabric model (MAT_058) [71]. The model was able to capture the load-displacement response, peak load and energy absorbed for various failure modes fairly accurately [71].

The built-in LS-DYNA material models have shown success when used to model unidirectional composites or laminated composites with unidirectional or fabric lamina. However, SMC materials, which have a lower fibre volume fraction and discontinuous fibre structure, exhibit a highly non-linear stress-strain response as the effect of the elasto-plastic matrix on the behaviour of the composite is more dominant, and therefore require a plasticity model which is absent in most of the available composite material models in LS-DYNA.

2.5 Pedestrian Safety Tests

In addition to the increased regulations in occupant safety, pedestrian safety is also becoming more important. The application of SMC materials to the exterior vehicle body panels also introduces the need to account for pedestrian safety in addition to structural performance of the panel.

In order to evaluate the ability of a vehicle component to protect pedestrians in the case of an impact, vehicle assessment programs, such as the European New Car Assessment Program (Euro NCAP) [72] and the Australasian New Car Assessment Program (ANCAP) [73], use impactors to represent the parts of the human body which will be impacted by the vehicle body.

The vehicle bonnet and windscreen are most likely to impact the head of the pedestrian.

Therefore, the head injury criteria (HIC) is used to evaluate pedestrian safety in these areas [74]. The HIC is a measure of the amount of acceleration of the center of gravity of the head and can be used to predict the probability of injury or death [75]. The panel is divided into multiple sections where the test will be conducted, with a headform impactor [74]. Some of these areas might pose a higher risk of injury due to proximity to surrounding vehicle components or difference in stiffness of the panel [74]. The HIC is calculated using equation 2.19, where A is the acceleration of the center of gravity of the head and T_1 and T_2 are two points in time, within 15 ms of one another, during the impact [75]. A HIC of 1000 is the threshold, above which would result in death [75].

$$HIC = max \left[\frac{1}{T_2 - T_1} \int_{T_1}^{T_2} A dT \right]^{2.5} (T_2 - T_1) \tag{2.19}$$

Studies involving simulation of the impact between a vehicle hood and head impactor exists in literature. Teng et al. found from simulating the head and hood impact test that the stiffness of the hood and the design of the hood reinforcements play a large role in determining the acceleration experienced by the headform impactor [75]. The design of the reinforcement structure has a large effect on the rate of directional change of the head which results in a larger overall acceleration [75]. Apart from that, generally a lower stiffness of the hood results in a lower acceleration experienced by the head [75]. Similar trends were observed in literature in studies by Ramesh et al. [76] and Masoumi et al. [77].

Ramesh et al. performs a redesign of a vehicle hood stiffener structure to meet the Euro NCAP regulations, where a reduction of the HIC was achieved by decreasing the local stiffness of the reinforcing structure, while maintaining a similar global stiffness to the baseline design [76].

Masoumi et al. compares the performance of a hood design made from steel, aluminum and composite in terms of strength and HIC [77]. The composite hood resulted in the lowest HIC and the highest deflection of the hood, this is followed by aluminum and finally steel [77]. This difference is likely due to the lower stiffness of the composite and aluminum hoods compared to the steel hood, since the same geometry was used for all three materials [77]. The lower the HIC the better it is for pedestrian safety. The deflection on the other hand, depends on the distance between the hood and the vehicle components under the hood [77].

Composite components used in vehicles are designed according to various load cases for passenger or pedestrian safety that will have to be simulated during component development. In order to be able to model these complex load cases, the material model in this

thesis has to be able to capture the fundamental behaviour of the composite in simpler load cases, such as standardized material tests for composites in tension, compression, in-plane shear and three-point bending.

2.6 Composite Testing

The impact of a vehicle body panel is a complex combined load case, which can consist of tension, compression, shear and bending. In order to evaluate the impact properties of composite materials without the use of a full vehicle body panel geometry, simplified standardized testing can be performed. One of the most widely used tests for this is drop-weight impact testing, where a plate specimen which is clamped or simply supported by a fixture and impacted with a weighted impactor [78, 79, 80, 81, 82, 83]. The ASTM D7136 standard test method is commonly used to measure the impact performance of FRP composites [82, 83]. A flat rectangular composite plate specimen is clamped to a support fixture with a rectangular unsupported region where the impact occurs. The impact energy is determined by the impactor mass and height from which the impactor is dropped. During this test, the force exerted by the impactor on the specimen and impactor velocity may be measured [84].

One of the most widely used standardized tensile test for composites is ASTM D3039 [80, 85, 86, 87, 88, 89, 90, 91, 92]. This test involves the use of a rectangular specimen with a uniform rectangular cross section, which is clamped at each end and loaded in tension. During this test, the force exerted, strain and displacement can be recorded to obtain the stress-strain response of the composite in tension [1].

From reviewing literature, there appeared to be a variety of methods of used to measure the compressive properties of a composite. Earlier works, used test standards for rigid plastics such as ASTM D695 [93]. Others [85, 93] have used ASTM D3410 which transfers load from the clamping fixture to the specimen through shear-loading [94], while ASTM D695 transfers load through end-loading [95]. A third standard method of testing composites is ASTM D6641 [96, 90, 97] which is a combined shear and end loading compressive test using a combined loading compression test fixture, which addresses some of the deficiencies in the previous two methods [2, 96]. Composites tested using ASTM D695 tended to fail due to the crushing of the ends, while using ASTM D3410 tended to require significant clamping force, which may damage the specimen, in order to prevent slippage and transfer load to the specimen effectively [96].

There is a large variety of in-plane shear testing methods available. Lee et al. compares the various methods of in-plane shear testing on composites [98]. Using the main criteria of

cost and accuracy, it was determined that the 45° tensile test and Iosipescu methods were the optimal methods of testing composites in in-plane shear loading [98]. The Iosipescu method, uses a specimen with V-shaped notches at the centerline. Forces are applied using a test fixture to generate two counteracting moments, to create an area of maximum pure shear stress at the centerline of the specimen [98]. Walrath et al. performs testing on a variety of composite material using the Iosipescu shear test noting similar advantages as Lee et al. had shown [99]. Adams et al. used the Iosipescu test method to measure the shear properties of SMC composite materials [100]. It is difficult to manufacture thin-walled tube specimens, which researchers agree is the most accurate method of measuring in-plane shear [98, 100], from SMC composites, hence the Iosipescu method is desirable in the testing of SMC composite. A standardized test method based on the Iosipescu method is ASTM D5379 [3].

Flexure testing, specifically three-point bending is typically performed according to ASTM D790 or ISO 178 [91, 101, 85, 92, 102, 103, 104]. In these standard tests, a rectangular specimen with a rectangular cross section is simply supported at two points and loaded at the midpoint between the supports with a loading nose. The deflection of the specimen at the midpoint is measured along with the force exerted, which will then be used to calculate the flexure stress and strain [105, 4].

In conclusion, there are standardized tests available, which have been used in literature, to characterize the behaviour of composite materials. However, there does not exist in literature a complete set of material data to fully characterize the behaviour of an SMC material. Therefore, this work will include the results of experimental testing performed by Dr. Julie Lévesque, from Laval University, Anna Trauth, from the Karlsruhe Institute of Technology, and General Motors as per standardized test specifications used in literature for composite materials. In order to ensure that the material model implemented in this thesis accurately captures the fundamental behaviour of the SMC material, the tensile, compressive, in-plane shear and three-point flexure tests are simulated and compared to the experimental results. The tensile, compressive and in-plane shear tests are used to calibrate the model while the flexure test is used to validate the model.

Chapter 3

Experimental Testing

This chapter covers the previous quasi-static experimental testing conducted on glass fibre reinforced polymer SMC plaques. Standardized testing had been previously performed for uniaxial tension, compression, in-plane shear and three-point bending. The tensile and compressive tests were performed by Dr. Julie Lévesque, from Laval University. The in-plane shear tests were performed by General Motors. The three-point flexure tests were performed by Anna Trauth, from the Karlsruhe Institute of Technology. The tests performed are quasi-static at strain rates $10^{-2}/s$ and below. Using the provided experimental stress-strain curves for each specimen in each test, the average stress-strain curve for each test is calculated and the behaviour of the composite is analysed. The calculated average stress-strain curves are used to calibrate and validate the material model implemented in the later sections.

3.1 Material Composition and Processing

The SMC plaques from which the test specimens were obtained is a glass fibre reinforced polyester. In addition, the polyester matrix also contains styrene and filler material such as glass spheres and calcium carbonate. The fibre volume fraction is approximately 18.3%. The SMC plaques were moulded from SMC charges manufactured by adding randomly oriented chopped glass fibres, which have a fibre length of approximately 1 in, in between two layers of matrix material. The charges were compression moulded and cured at $150°C$ for several minutes to create finished plaques in the form of sheets. The moulding process can result in defects, such as voids in the material or discontinuities in reinforcement where two flow fronts merge.

The tests for tension, compression and bending were conducted in both the 0° and 90° directions, which are aligned and perpendicular to the flow direction of the material during the moulding process respectively. The material directions are defined in Figure 3.1.

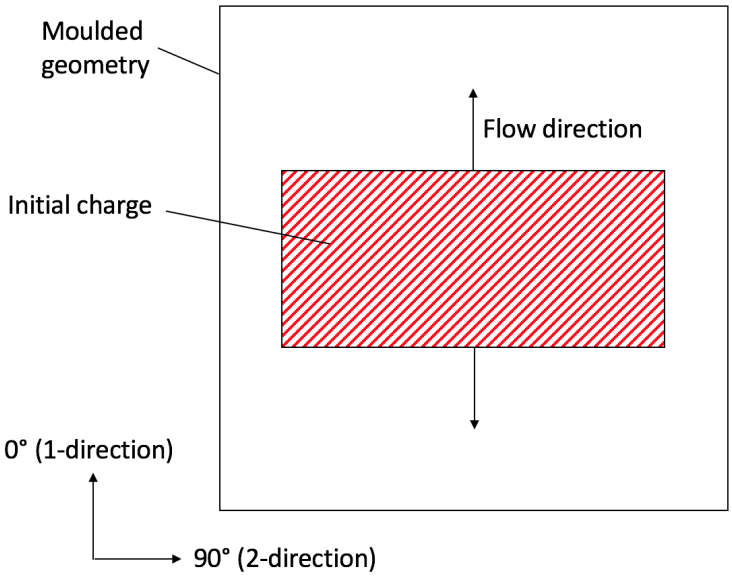

Figure 3.1: Illustration of a moulded SMC plaque showing the material directions with respect to the flow direction during moulding

3.2 Tensile Testing

Tensile testing was performed according to ASTM D3039 [1] by Dr. Julie Lévesque from Laval University. Tensile testing was performed in the 0° and 90° directions to measure the in-plane anisotropy of the composite under a tensile load. The tensile testing specimens are rectangular specimens with the dimensions given in Table 3.1. The specimens were clamped in a tensile testing fixture with one end fixed, while the other end was loaded at 2 mm/min in the tensile direction. The strain was measured using digital image correlation (DIC). The test was performed for three specimens in each direction. The stress-strain curves for the uniaxial tensile test in the 0° and 90° directions are shown in Figures 3.2 and 3.3 respectively. The average stress-strain curves, represented by the solid lines, are calculated from the raw experimental results, represented by the dashed lines, up to the minimum failure strain. The Lankford coefficients or r-values for the tensile test are calculated from

the measured transverse and longitudinal strains to be 0.397 and 0.387 for the 0° and 90° directions respectively. These values are used in the calibration of the yield function.

Table 3.1: Tensile testing specimen dimensions [1]

Parameter	Value, mm
Overall length	250
Width	25
Grip length	37.5
Thickness	2.4

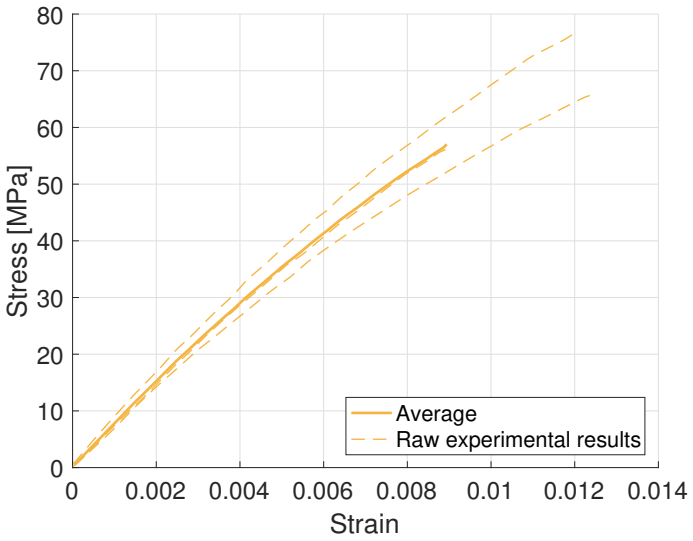

Figure 3.2: Experimental stress-strain response for tension in the 0° direction

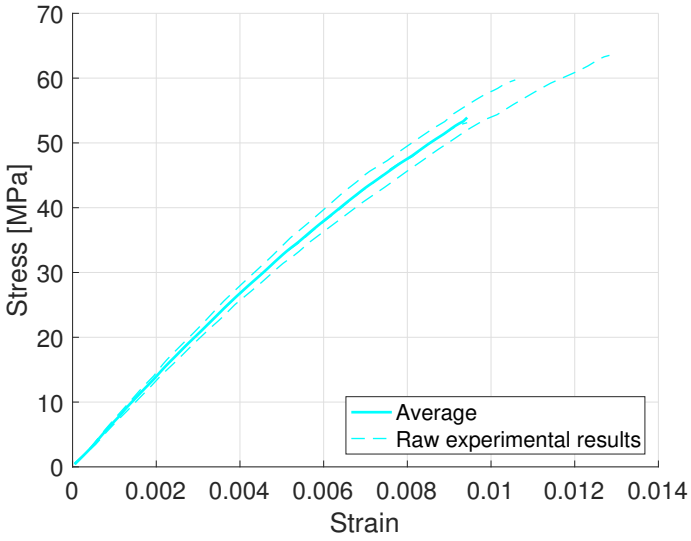

Figure 3.3: Experimental stress-strain response for tension in the 90° direction

3.3 Compressive Testing

The compressive testing was performed according to ASTM D6641 [2] by Dr. Julie Lévesque from Laval University. The test performed is a combined loading compression test, where both an end and shear load is applied to the specimen in order transfer load to the specimen effectively without damaging the gripped areas. The compressive test specimens are rectangular specimens with the dimensions given in Table 3.2. The gripped faces were reinforced by aluminum tabs, attached using a two-part epoxy, to eliminate failure within the gripping fixture. The axial strains were measured on both sides of the specimen using strain gauges attached to each side of the specimen. This allows the strains on each side to be compared to verify that the specimen was not buckling during testing. The specimens were loaded at 1 mm/min in the compressive direction. The compressive test was performed for three specimens in the 0° and 90° directions. The results of two specimens in the 0° direction and one specimen in the 90° direction were invalid, according to the test specification, and rejected as the strain measured on each face of the specimens differed significantly due to buckling in the gauge region. The remaining experimental results for the compressive test in the 0° and 90° directions are shown in Figures 3.4 and 3.5 respectively. The average stress-strain curves, represented by the solid lines, are calculated

from the raw experimental results, represented by the dashed lines, up to the minimum failure strain. In Figure 3.4, the average and raw experimental result is the same curve as there is only one valid result.

Table 3.2: Compressive testing specimen dimensions [2]

Parameter	Value, mm
Overall length	140
Width	12
Untabbed length	13
Strain gauge length	2
Thickness	2.4

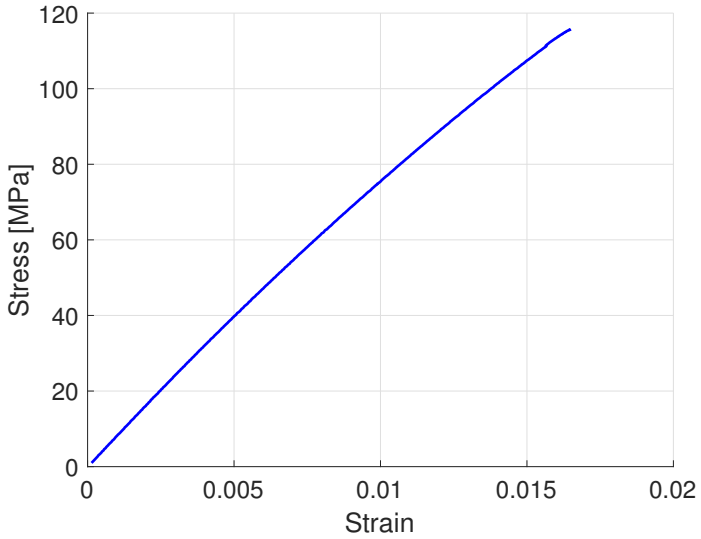

Figure 3.4: Experimental stress-strain response for compression in the 0° direction

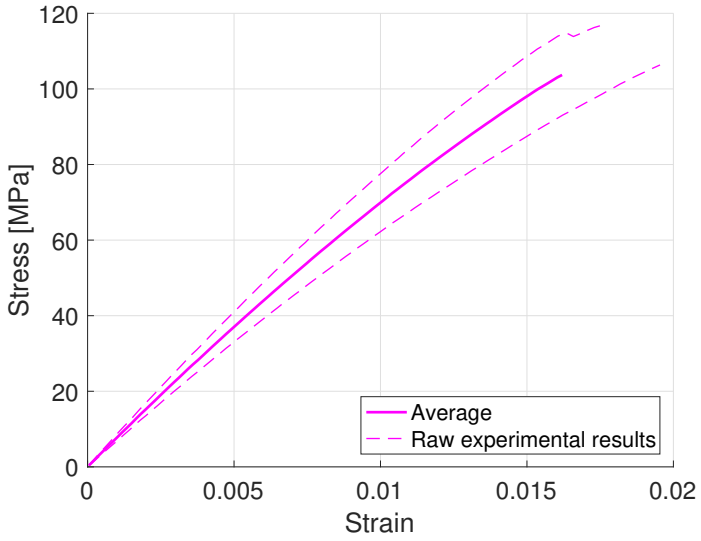

Figure 3.5: Experimental stress-strain response for compression in the 90° direction

3.4 In-Plane Shear Testing

In-plane shear testing was performed according to ASTM D5379 [3] by General Motors. In this test, forces were applied to the specimen in opposing directions through a loading fixture to generate an area of maximum shear stress at the center of the specimen [98]. The specimens used are rectangular specimens with 90° V-notches at the centerline [3]. The dimensions of the specimens are given in Table 3.3. DIC was used to obtain the in-plane shear strain of the specimen. The specimens were loaded at 1.5 mm/min. The in-plane shear test was performed for three specimens and the results are shown in Figure 3.6. The average stress-strain curves, represented by the solid lines, are calculated from the raw experimental results, represented by the dashed lines, up to the minimum failure strain.

Table 3.3: Shear testing specimen dimensions [3]

Parameter	Value, mm
Gauge section width	11.21
Thickness	3.49
Gauge length	2.5
Notch radius	1.3
Length	76
Overall width	19

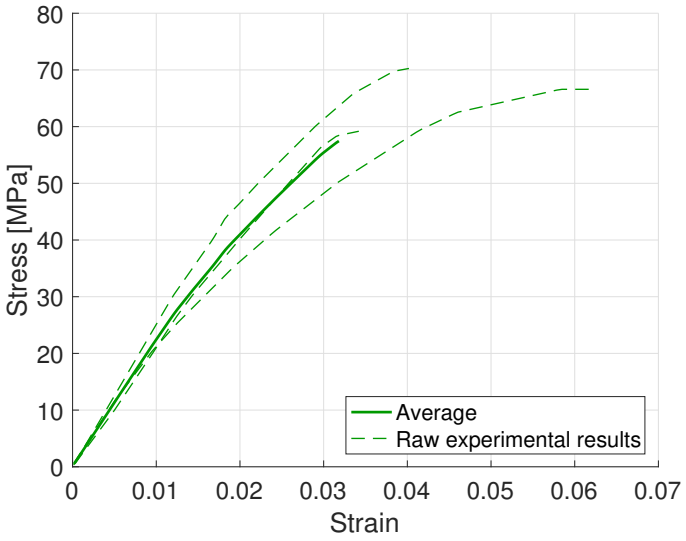

Figure 3.6: Experimental stress-strain response for in-plane shear

3.5 Flexure Testing

The three-point bend or flexure testing, in the 0° and 90° directions of the moulded SMC plaque, was performed according to DIN EN ISO 178 [4] by Anna Trauth from the Karlsruhe Institute of Technology. In this test, a rectangular specimen was supported by two supports, while a load was applied by a loading fixture at the center of the specimen in the through-thickness direction [4]. The specimen and fixture dimensions are given in Table 3.4. The specimens were loaded at 1 mm/min in the vertical direction. Results were obtained for 19 specimens in the 0° direction and 10 specimens in the 90° direction.

Table 3.4: Flexure testing specimen and fixture dimensions [4]

Parameter	Value, mm
Thickness, d	2.7
Width, b	10
Support length, L	58
Loading fixture radius	5
Support fixture radius	2

The flexure strain and stress are calculated with equations 3.1 and 3.2 respectively [4]. The variables D and P are the deflection at the center of the specimen and the load applied by the loading fixture respectively.

$$\varepsilon_{flexure} = \frac{6Dd}{L^2} \tag{3.1}$$

$$\sigma_{flexure} = \frac{3PL}{2bd^2} \tag{3.2}$$

Figures 3.7 and 3.8 shows the stress-strain curves for the flexure test in the 0° and 90° directions. The average stress-strain curves, represented by the solid lines, are calculated from the raw experimental results, represented by the dashed lines, up to the minimum failure strain.

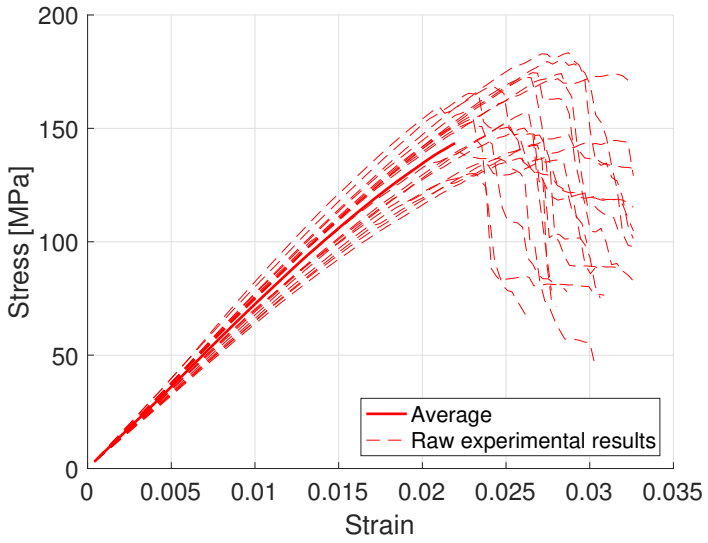

Figure 3.7: Experimental stress-strain response for flexure in the 0° direction

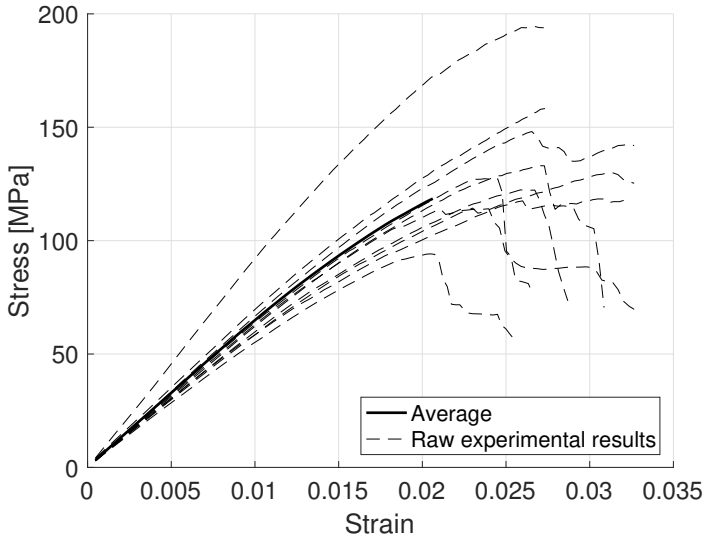

Figure 3.8: Experimental stress-strain response for flexure in the 90° direction

3.6 Discussion of Experimental Results

The average experimental stress-strain curves for the tensile and compressive tests in the 0° and 90° directions, calculated from the raw experimental results provided by Dr. Julie Lévesque from Laval University, are compared in Figure 3.9 to determine the behaviour of the SMC composite in various loading directions. From the comparison, it is evident that tension-compression asymmetry in present in both the 0° and 90° directions, where the material is stiffer in compression than tension for both loading directions. In addition, in-plane anisotropy is also observed between the 0° and 90° directions, the material is stiffer in the 0° direction in both tension and compression. As suggested by literature, the anisotropy is caused by the slight orientation of the fibres induced by the manufacturing process of the composite [19, 20]. Both the elastic and plastic regime are anisotropic and asymmetric in tension and compression. The tensile tests also fail at a significantly lower strain compared to the compressive tests, this is due to a difference in failure mode in tension and compression. In-plane anisotropy is also observed in the flexure experiments, this is shown in Figure 3.10 which compares the average flexure stress-strain curves in the 0° and 90° directions, calculated from the raw experimental results provided by Anna Trauth from the Karlsruhe Institute of Technology. Overall, the material behaviour of this SMC composite, which includes the stiffer response in compression than tension and the presence of in-plane anisotropy, is similar to the behaviour observed in literature.

Apart from the insight into the material behaviour, the experimental results also show the variation in properties within the composite. A significant variation in stress-strain behaviour is observed in the raw experimental curves. This is likely due to the manufacturing process, which can result in a non-uniform fibre volume fraction distribution and orientation distribution in the composite material. The variation in behaviour can also be due to the presence of defects, such as voids, in some areas of the plaque.

The existing set of experimental data are for tests performed using specimens with dimensions as per the standardized test specifications. In the future, it would be beneficial to perform the experiments for a range of specimens, with various lengths and widths, to determine the sensitivity of the measured results to the specimen dimensions with respect to the fibre length.

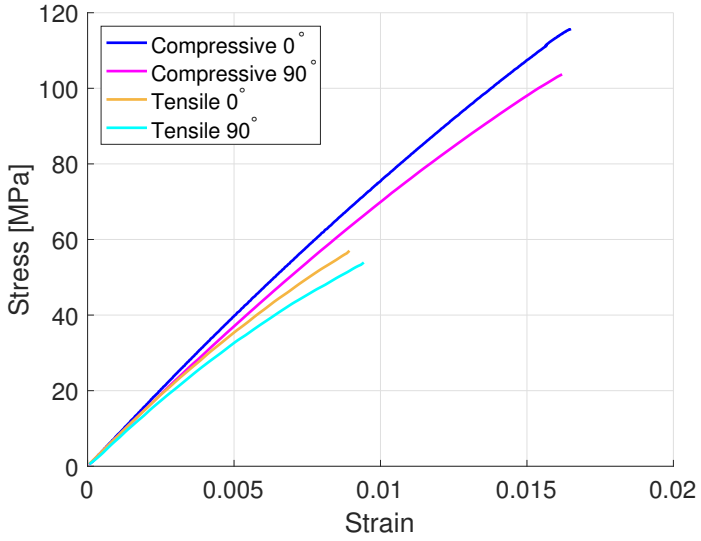

Figure 3.9: Comparison between experimental stress-strain curves for tension and compression in the 0° and 90° directions

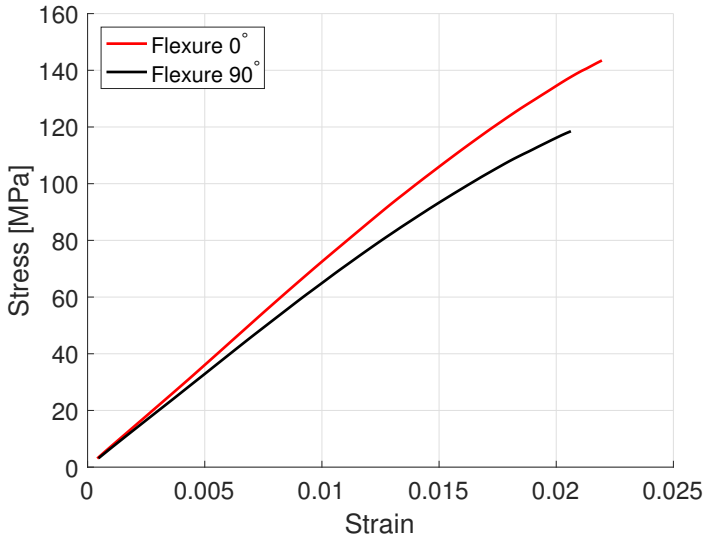

Figure 3.10: Comparison between experimental stress-strain curves for flexure in the 0° and 90° directions

Chapter 4

Material Model Implementation

A non-linear elasto-plastic material model for explicit analysis is implemented in order to capture the complex behaviour of the SMC composite observed in experimental results. A forward Euler integration scheme is used in the SMC material model. The model is implemented in the FEA solver, LS-DYNA.

4.1 Elastic Model

In order, to capture the in-plane anisotropy due to the orientation of the chopped glass fibres, the orthotropic elastic stiffness tensor introduced in Section 2.4.1 is required. It is calculated using equations 4.1 and 4.2, where E are the elastic moduli, G are the shear moduli and v are the Poisson's ratios [50]. It is orthotropic with respect to the 0° and 90° directions. The 0° direction, 90° direction and through-thickness direction are aligned with the 1, 2 and 3-directions respectively.

$$\mathbb{L}_{el} = \begin{bmatrix} \frac{1-v_{23}v_{32}}{E_2E_3\Delta} & \frac{v_{21}+v_{31}v_{23}}{E_2E_3\Delta} & \frac{v_{31}+v_{21}v_{32}}{E_2E_3\Delta} & 0 & 0 & 0 \\ \frac{v_{12}+v_{13}v_{32}}{E_3E_1\Delta} & \frac{1-v_{31}v_{13}}{E_3E_1\Delta} & \frac{v_{32}+v_{31}v_{12}}{E_3E_1\Delta} & 0 & 0 & 0 \\ \frac{v_{13}+v_{12}v_{23}}{E_1E_2\Delta} & \frac{v_{23}+v_{13}v_{21}}{E_1E_2\Delta} & \frac{1-v_{12}v_{21}}{E_1E_2\Delta} & 0 & 0 & 0 \\ 0 & 0 & 0 & 2G_{12} & 0 & 0 \\ 0 & 0 & 0 & 0 & 2G_{23} & 0 \\ 0 & 0 & 0 & 0 & 0 & 2G_{31} \end{bmatrix} \tag{4.1}$$

$$\Delta = \frac{1 - v_{12}v_{21} - v_{23}v_{32} - v_{31}v_{13} - 2v_{12}v_{23}v_{31}}{E_1E_2E_3} \tag{4.2}$$

In order to capture the tension-compression asymmetry in the elastic behaviour of the composite, the stress triaxiality, T, is used to determine if the material is in tension or compression. Stress triaxiality is calculated using equation 4.3, where I_1 and J_2 are calculated using equations 4.4 and 4.5 respectively. σ is the stress, while $\mathbf{S}$ is the deviatoric stress, calculated using equation 4.6. A simple criterion is implemented where the material is considered to be in compression if the triaxiality is negative, and tension if it is positive. The components of the elastic stiffness matrix for the normal directions are assigned either the tensile modulus or compressive modulus depending on the triaxiality for the current stress state.

$$T = \frac{I_1}{3\sqrt{3J_2}} \tag{4.3}$$

$$I_1 = \sigma_1 + \sigma_2 + \sigma_3 \tag{4.4}$$

$$J_2 = \frac{1}{2}\mathbf{S} : \mathbf{S} \tag{4.5}$$

$$\mathbf{S} = \sigma - \frac{1}{3}I_1 \tag{4.6}$$

4.2 Yield Function

Based on the experimental results, there is an observed tension-compression asymmetry and in-plane anisotropy in yielding. Therefore, a yield criterion capable of capturing this behaviour is required. The orthotropic yield criterion developed by Cazacu et al. [60], introduced in Section 2.4.2 and shown in equation 4.7, is selected for this purpose over the pressure dependent yield criteria studied by Donato et al. [25] which only capture the tension-compression asymmetry. The orthotropic yield criterion by Cazacu et el. is able to capture orthotropic yielding through a linear transformation of the deviatoric stress tensor, shown in equation 4.8, with the transformation tensor in equation 4.9, while tension-compression asymmetry is captured through the k parameter in equation 4.7.

$$(|\Sigma_1| - k \cdot \Sigma_1)^a + (|\Sigma_2| - k \cdot \Sigma_2)^a + (|\Sigma_3| - k \cdot \Sigma_3)^a = F^a \tag{4.7}$$

$$\Sigma = \mathbb{C} : \mathbf{S} \tag{4.8}$$

$$\mathbb{C} = \begin{bmatrix} C_{11} & C_{12} & C_{13} & 0 & 0 & 0 \\ C_{12} & C_{22} & C_{23} & 0 & 0 & 0 \\ C_{13} & C_{23} & C_{33} & 0 & 0 & 0 \\ 0 & 0 & 0 & C_{44} & 0 & 0 \\ 0 & 0 & 0 & 0 & C_{55} & 0 \\ 0 & 0 & 0 & 0 & 0 & C_{66} \end{bmatrix} \tag{4.9}$$

4.3 Hardening Model

Apart from the yield criterion, a hardening rule is also required to model how the material hardens as yielding occurs by relating the effective plastic strain to the flow stress. The hardening rule determines how the yield surface expands with respect to the effective plastic strain [51]. A power law hardening rule is used to capture the hardening behaviour of the SMC composite. The version of power law hardening rule used is Ludwik's equation [62], introduced in Section 2.4.3 and given in equation 4.10, where $\bar{\sigma}$ is the flow stress, σ_y is the yield stress, $\bar{\varepsilon}_p$ is the effective plastic strain, K is the strength coefficient and n is the strain hardening exponent [62].

$$\bar{\sigma} = \sigma_y + K(\bar{\varepsilon}_p)^n \tag{4.10}$$

4.4 Stress Integration Algorithm

The material model is based on a forward Euler integration scheme. The stresses and effective plastic strain at each time step of the simulation, for each element, is evaluated based on the algorithm proposed by Williams et al. [106, 107]. Based on the boundary conditions, the strain increment is provided as an input by the LS-DYNA solver for each element. The stress at the end of the time step is given by equation 4.11, where $\mathbb{L}_{el}$ is the elastic stiffness tensor, $d\varepsilon$ is the strain increment and $d\varepsilon_p$ is the plastic strain increment. The plastic strain increment is 0 at the beginning of the time step.

$$\sigma_{n+1} = \sigma_n + \mathbb{L}_{el} : (d\varepsilon - d\varepsilon_p) \tag{4.11}$$

The plastic strain increment is calculated using the associative flow rule shown in equation 4.12, where $d\lambda$ is a plastic multiplier, which is equal to the increment in effective plastic strain [108], and $\partial\phi/\partial\sigma$ is the normal to the yield surface, which is the derivative of the yield criterion, ϕ, with respect to the Cauchy stress.

$$d\varepsilon_p = d\lambda \frac{\partial \phi}{\partial \sigma} \tag{4.12}$$

The yield criterion shown in equation 4.13 is used to determine if yielding has occurred. F is the effective stress calculated using the orthotropic yield function given in equation 2.14 and $\bar{\sigma}$ is the flow stress at the current effective plastic strain calculated using the hardening rule given in equation 2.17.

$$\phi = F - \bar{\sigma} \tag{4.13}$$

If the effective stress exceeds the flow stress for the current amount of plastic strain, an iterative loop using the Convex Cutting Plane (CCP) algorithm introduced by Abedrabbo et al. [109] is required to determine the amount of plastic strain resulting from the current strain increment, and enforce the yield criterion. The stress and plastic strain during each iteration of this loop, indicated by the subscript s, is given by equations 4.14 and 4.15 respectively, where $\bar{\varepsilon}$ is the effective plastic strain. $\Delta\partial\lambda$ is an update to the effective plastic strain increment and is calculated based on the equation 4.16. $\partial\phi/\partial\sigma$ is the derivative of the yield criterion with respect to the Cauchy stress, while $\partial\bar{\sigma}/\partial\bar{\varepsilon}$ is the derivative of the flow stress expression with respect to the effective plastic strain.

$$\sigma_{s+1} = \sigma_s - (\Delta d\lambda_s)\mathbb{L}_{el} : \frac{\partial \phi}{\partial \sigma} \tag{4.14}$$

$$\bar{\varepsilon}_{s+1} = \bar{\varepsilon}_s + \Delta d\lambda_s \tag{4.15}$$

$$\Delta d\lambda = \frac{\phi}{\frac{\partial \phi}{\partial \sigma} : \mathbb{L}_{el} : \frac{\partial \phi}{\partial \sigma} + \frac{\partial \bar{\sigma}}{\partial \bar{\varepsilon}}} \tag{4.16}$$

Using this prediction of the stress and plastic strain, the yield criterion is re-evaluated to determine if the effective stress matches the flow stress. This loop repeats until the absolute difference between the effective stress and flow stress is less than or equal to 10^{-8}.

4.5 Limitations

This model assumes that all non-linearity in the material's stress-strain response is due to plasticity and ignores the stiffness reduction due to damage. The use of the current model is acceptable for the current set of load cases due to the monotonic loads. Cyclic testing can be performed to determine the relative contribution of plasticity and damage to the material non-linearity.

Another limitation of the current model is that it does not account for strain rate effects. Current testing is performed at quasi-static strain rates. If the model is to be applied to higher strain rates, a strain rate sensitivity term, similar to the strain rate term in the Johnson-Cook hardening model, can be added to the current hardening function and calibrated to experiments at several different strain rates.

4.6 User-Defined Material Model

For the above material model to be used for component level finite element simulation, it has to be implemented as a user-defined material model in a finite element software. In this case, LS-DYNA is the finite element software selected. Figure 4.1 shows how the material model interacts with the LS-DYNA solver. σ_n, $\bar{\varepsilon}^p_n$ and $d\varepsilon$ are the current stress, effective plastic strain and the strain increment respectively, which are the inputs to the user-defined material model. $sigma_{n+1}$ and $\bar{\varepsilon}^p_{n+1}$ are the stress and effective plastic strain at the beginning of the next time step, output by the material model. ϕ is the yield criterion. The user-defined material model is used in finite element simulations of the tensile, compressive and in-plane shear test to calibrate the material parameters to the experimental results. The calibrated material model is then used to predict the flexure response of the SMC composite.

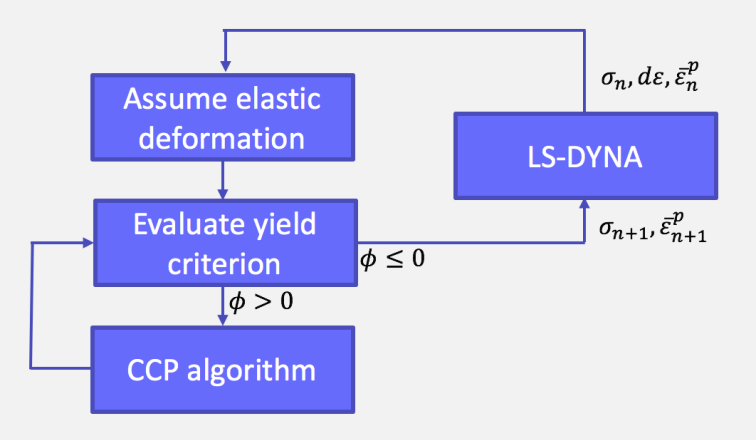

Figure 4.1: LS-DYNA user-defined material model framework

Chapter 5

Numerical Simulations

The goal for the model is to accurately predict the flexural response of the SMC composite by accounting for the in-plane anisotropy and tension-compression asymmetry observed in experiments. Before the model can be used to predict the flexure response, the model will have to be calibrated to determine, the elastic moduli, hardening parameters and yield function parameters.

The material model is calibrated using an iterative inverse finite element analysis approach, where the stress-strain response from component level simulations is compared to the experimentally measured data to obtain the material model parameters required to capture the observed material behaviour. This method of calibration most closely reproduces the experimental results as it is able to account for the boundary effects in tests such as the compressive test. However, this comes at the cost of longer lengths of time required to calibrate the model.

The user-defined material model is used to perform simulations of the tensile, compressive and in-plane shear in order to calibrate the model parameters to the experimental tensile, compressive and in-plane shear test results. The calibrated user-defined material model is then validated by using it to perform flexure test simulations.

5.1 Finite Element Model Setup

In order to model the physical tests as accurately as possible, the finite element model of the tests should reflect the dimensions and boundary conditions of the physical tests as closely as possible. This section explains the finite element model for each test in detail.

Calibration is performed using the tensile, compressive and in-plane shear tests, while the model predictions for the flexure tests are used to validate the material model.

All finite element models discussed in this section use the LS-DYNA element formulation 2, a selectively reduced fully integrated solid element. An attempt is made to ensure the aspect ratio of the elements is approximately 1, but this is not possible due to the mesh refinement in some areas, while using only hexahedral elements. The finite element mesh for the tensile, compressive, in-plane shear and flexure specimen are shown in Figures 5.1, 5.2, 5.3 and 5.4 respectively. Symmetry boundary conditions, represented by the planes shown the figures, are used to reduce the size of the mesh and reduce the amount of computational resources required. Symmetry boundary conditions are boundary conditions applied to the nodes, which lie on the symmetry planes, that constrain the nodes to the plane of symmetry. For example, a symmetry boundary condition for the xy-plane constrains the nodes on the plane in the translational degree of freedom along the z-axis, and the rotational degrees of freedom about the x and y-axis.

5.1.1 Tensile Test Model Setup

The specimen geometry for the tensile test are the dimensions given in Table 3.1. There are two elements across the thickness of the specimen. An eighth symmetry model is used for the tensile test model. The model is symmetric about the xy-plane, yz-plane and xz-plane. The gripped faces of the specimen are prescribed a tensile velocity in the axial direction and fixed in the transverse direction to reflect the constraints imposed by the stationary and loading grippers of the tensile testing apparatus. The velocity applied is halved, to account for the symmetry boundary conditions, and time scaled by a factor of 1000, to reduce computation time. The finite element mesh and boundary conditions applied are shown in Figure 5.1. The mesh consists of 1040 elements, each approximately 1.2 mm in size.

5.1.2 Compressive Test Model Setup

The specimen geometry for compressive test are the dimensions given in Table 3.2. In addition to the SMC specimen, the aluminum tabs are modeled as well, using a linear elastic material model with the properties shown in Table 5.1. There are four elements across the thickness of the SMC specimen. Similar to the tensile test model, this model is an eighth symmetry model, symmetric about the xy-plane, yz-plane and xz-plane. The gripped and end faces of the specimen are prescribed a compressive velocity in the axial

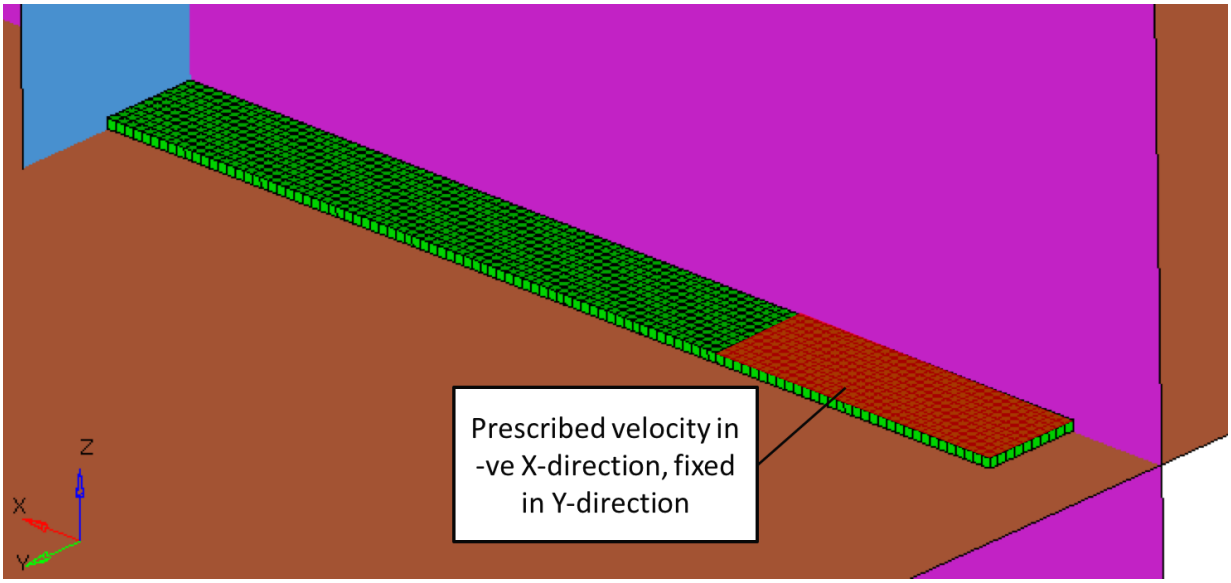

Figure 5.1: Finite element model for tensile test

direction and fixed in the transverse and through-thickness directions. The velocity applied is halved, to account for the symmetry boundary conditions, and time scaled by a factor of 100, to reduce computation time. The displacement is measured by the elongation of the gauge region in the loading direction. The finite element mesh and boundary conditions applied are shown in Figure 5.2. The mesh consists of 5520 elements, approximately 0.5 to 0.6 mm in size.

Table 5.1: Material properties for aluminum

Parameter	Value
Elastic Modulus	68.9 GPa
Poisson's Ratio	0.33
Density	2.7×10^{-3} g/mm^3

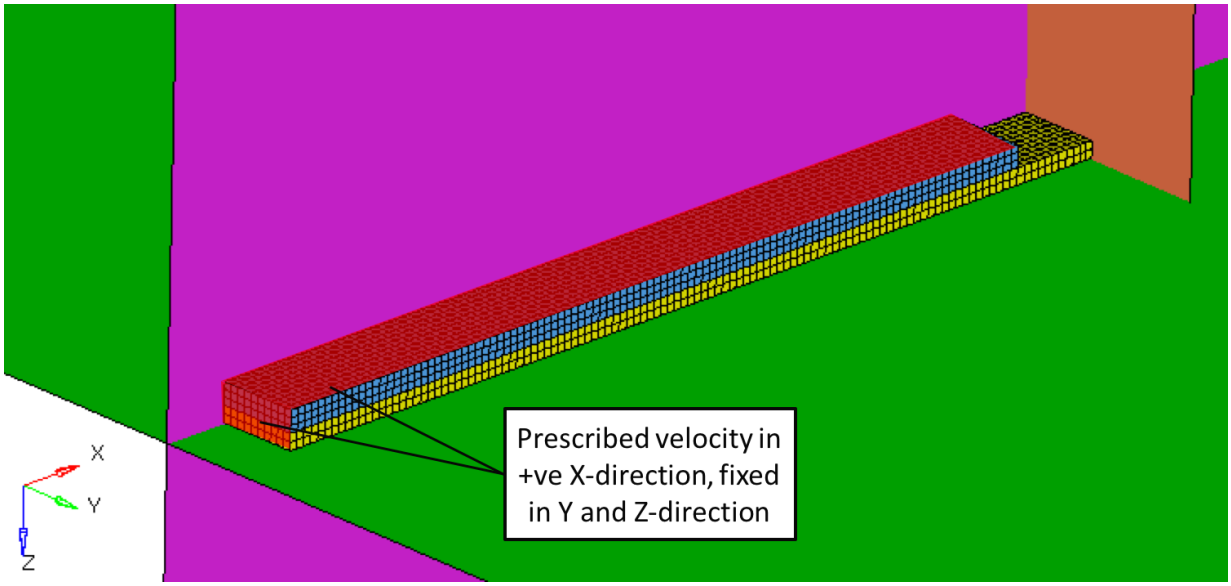

Figure 5.2: Finite element model for compressive test

5.1.3 Shear Test Model Setup

The specimen geometry for the in-plane shear test are the dimensions given in Table 3.3. There are twelve elements across the thickness of the in-plane shear specimen model. A half symmetry model about the xy-plane is used for the in-plane shear model. The gripped faces on the stationary end of the specimen are constrained in all translational degrees of freedom. The gripped faces on the loading end is constrained in the translational degrees of freedom along the x and z-direction and prescribed a velocity in the negative y-direction. The model is time scaled by a factor of 1000 to reduce computation time. The finite element mesh and boundary conditions applied are shown in Figure 5.3. The mesh consists of 40320 elements, ranging from approximately 0.1 to 0.5 mm in size, with finer elements near the notch radii.

5.1.4 Flexure Test Model Setup

The specimen geometry of the flexure test are the dimensions given in Table 3.4. Eight elements are used across the thickness of the flexure test specimen. The loading nose and supports are modeled using rigid linear hexahedral elements. A surface to surface contact is defined between the loading nose and the test specimen, and the supports and the test

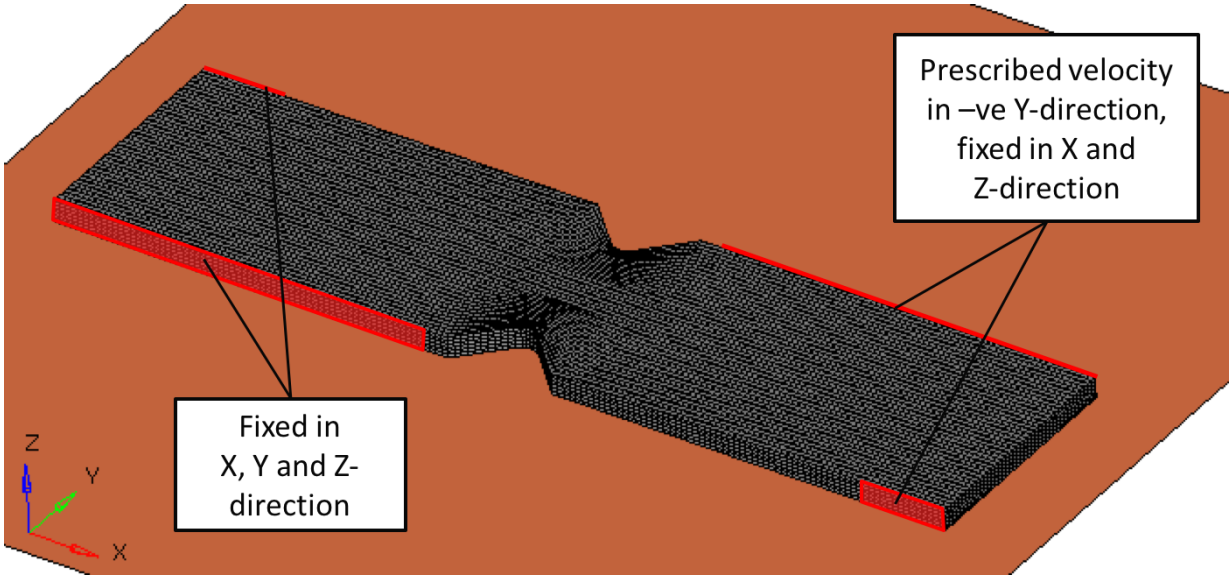

Figure 5.3: Finite element model for shear test

specimen. The coefficient of friction is 0.3 for both contact pairs. The finite element model used is a quarter symmetry model about the xz and yz-planes. The supports are fixed in all translational degrees of freedom, while the loading nose is fixed in the translational degrees of freedom along the x and y-direction and prescribed a velocity in the negative z-direction. The model is time scaled by a factor of 10000 to reduce computation time. The finite element mesh and boundary conditions are shown in Figure 5.4. The mesh consists of 14280 elements, approximately 0.333 mm in size.

5.2 Model Calibration Method

The power law hardening rule is calibrated to the stress versus plastic strain curve for uniaxial tension. Plastic strain is calculated from the experimental true strain using equation 5.1. The plastic strain calculated is plotted against the stress values and points along the curve are selected to calculate the hardening strength, hardening exponent and initial yield stress value. The calibrated flow stress curve is compared to the curve obtained from the uniaxial tensile experiment in Figure 5.5.

$$\bar{\varepsilon}_p = \varepsilon_{11} - \frac{\sigma_{11}}{E_1} \tag{5.1}$$

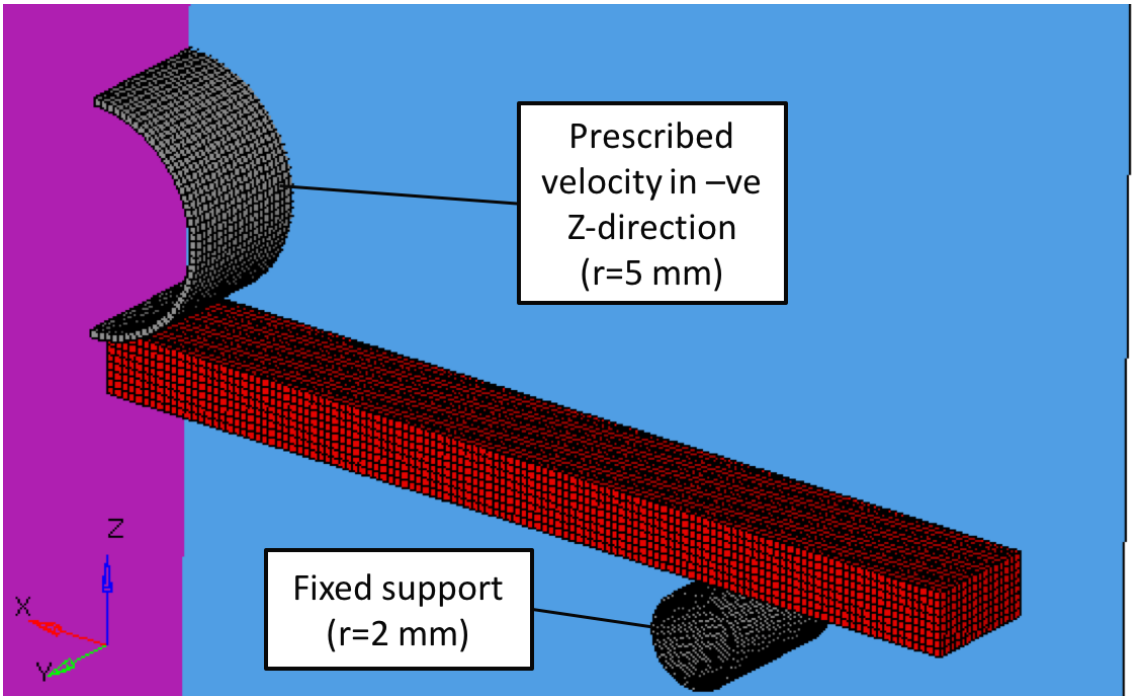

Figure 5.4: Finite element model for flexure test

Using the inverse finite element approach, the ratios between the yield points of each loading direction are adjusted. The required yield function parameters to maintain the selected ratios and selected Lankford coefficients or r-values are calculated using the Levenberg-Marquardt optimization algorithm [110, 111] in MATLAB. Due to unavailability of test data, it is assumed that, the elastic moduli $E_3 = E_2$, the shear moduli $G_{23} = G_{31} = G_{12}$, the r-values $r_{0C} = r_{0T}$ and $r_{90C} = r_{90T}$, and the shear orthotropy terms of the yield function transformation matrix $C_{55} = C_{66} = C_{44}$. The calibrated in-plane axial CPB yield surface is shown in Figure 5.6, where the horizontal axis is the stress in the 0° direction (σ_{11}), while the vertical axis is the stress in the 90° direction (σ_{22}). Both stresses are normalized with respect to the tensile yield stress in the 0° direction, (σ_{T0}). The following sections detail the finite element models used in the simulation of the tensile, compressive and in-plane shear tests.

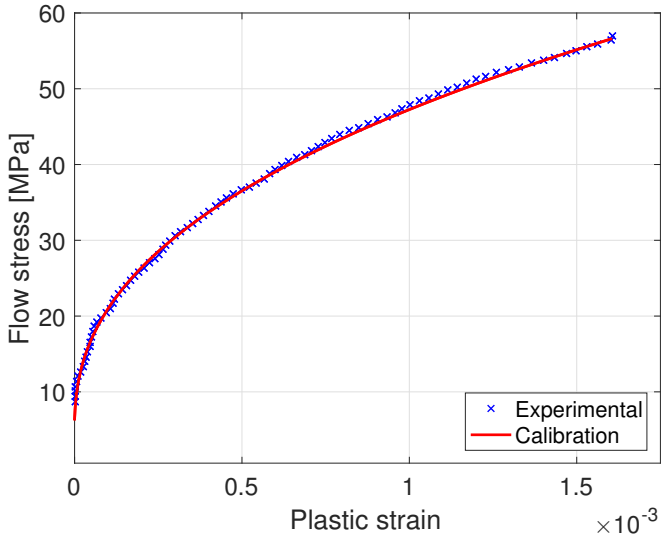

Figure 5.5: Calibrated versus experimental flow stress curve

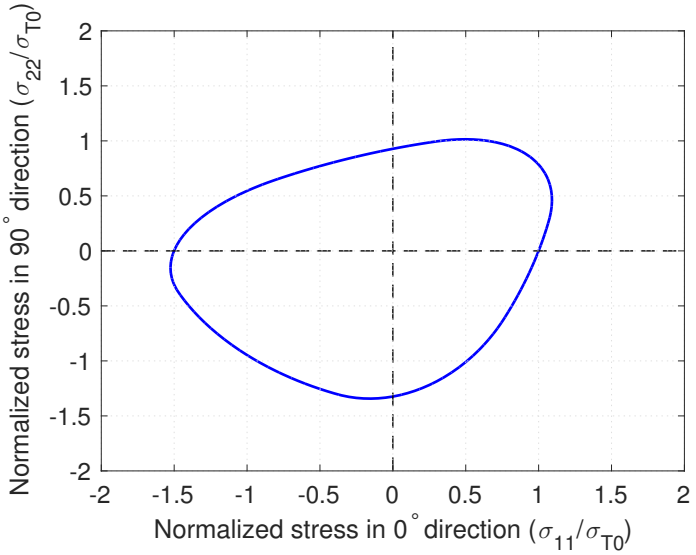

Figure 5.6: Calibrated CPB yield surface

5.3 Calibration Results

Using the finite element models detailed in the previous sections and the LS-DYNA solver, the SMC user-defined material model is calibrated against the average of the experimental stress-strain curves in Section 3.6. The elastic, hardening and yield function parameters are summarized in Tables 5.2, 5.3 and 5.4 respectively. The material 1-direction is aligned with the 0° direction while the material 2-direction is aligned with the 90° direction.

Table 5.2: Elastic parameters

Parameter	Value
Tensile Modulus (E_{1T})	7775 MPa
Tensile Modulus (E_{2T},E_{3T})	7150 MPa
Compressive Modulus (E_{1C})	8450 MPa
Compressive Modulus (E_{2C},E_{3C})	7950 MPa
Shear Modulus (G_{12},G_{23},G_{31})	2375 MPa
Poisson's Ratio (v_{12})	0.3

Table 5.3: Hardening parameters

Parameter	Value
Yield Stress (σ_y)	5 MPa
Power Law Hardening Strength (K)	782.89 MPa
Power Law Hardening Exponent (n)	0.4226

Figures 5.7, 5.8 and 5.9 compare the simulation results using the calibrated material model to the average experimental results for the tensile, compressive and in-plane shear load cases respectively. The implemented material model is able to successfully replicate the experimentally measured stress-strain behaviour for axial and shear loading. The relative error between the simulated tests and experimental tests for the calibration is shown in Figure 5.10, where the horizontal axis is the test progress, calculated by dividing the current strain by the strain at the end of the test. The Mean Absolute Errors (MAE) [112] for the calibration tests are within 1.5% of the experimental results.

Table 5.4: Yield function parameters

Yield function parameter	Value
k	-0.3665
a	2
C_{11}	1.2179
C_{22}	1.2590
C_{33}	0.9671
C_{12}	0.2961
C_{13}	0.0017
C_{23}	-0.0694
C_{44}	0.86
C_{55}	0.86
C_{66}	0.86

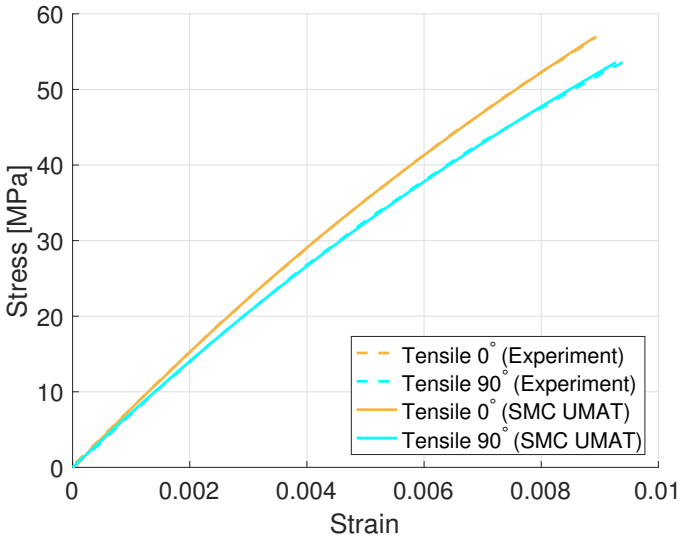

Figure 5.7: Calibrated stress-strain response for tensile test

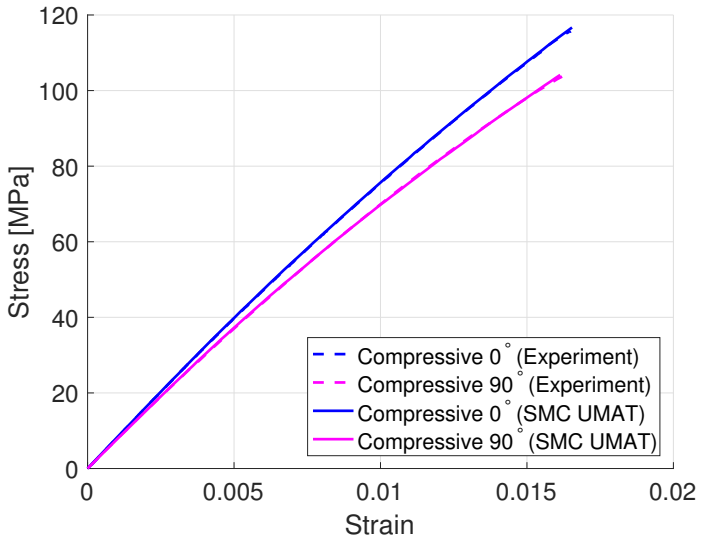

Figure 5.8: Calibrated stress-strain response for compressive test

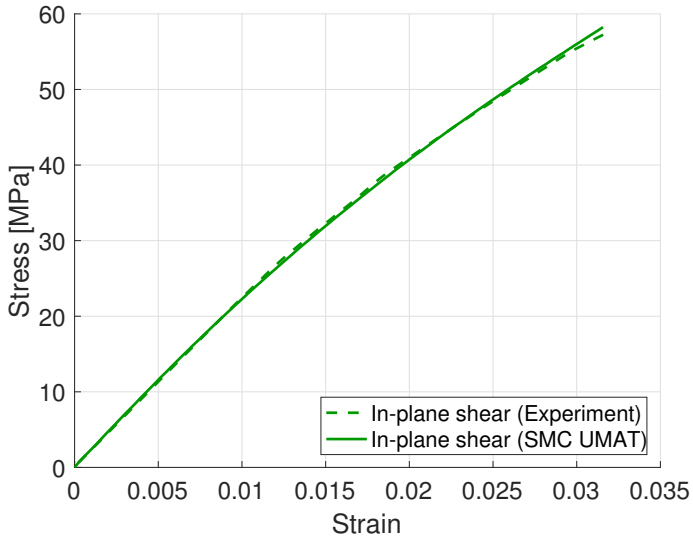

Figure 5.9: Calibrated stress-strain response for in-plane shear test

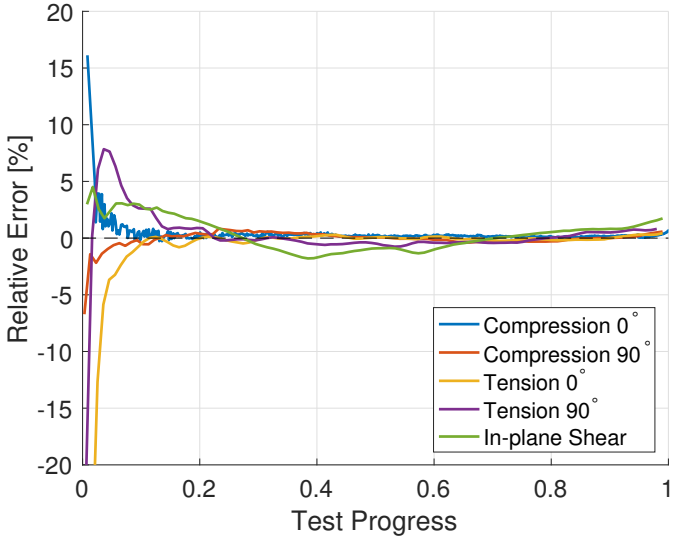

Figure 5.10: Error plot for calibration vs. experiment

5.4 Flexure Test Simulation Results

Using the material model calibrated to the experimental data for tension, compression and in-plane shear, the three-point flexure test is simulated using the model detailed in Section 5.1.4.

The simulation results for the flexure test are shown in Figure 5.11. The simulation overpredicts the flexure stress-strain response compared to the average experimental results for both the 0° and 90° directions. However, it is important to note that there is a large variation among the experimental flexure results and the predictions are within this variation. It is also to be noted that the relative stress-strain response between the both the 0° and 90° directions of the simulations is similar to the experimental results. The relative error of the predictions for the flexure tests are plotted against test progress in Figure 5.12. The dashed lines show the maximum and minimum variation of the experimental test results. The mean absolute errors are approximately 5% and 8% for the 0° and 90° directions respectively.

The predicted flexure response from the simulations shows an overprediction compared to the experimentally measured response. This difference in stress-strain responses could be due to various mechanisms which have not been accounted for or assumptions made.

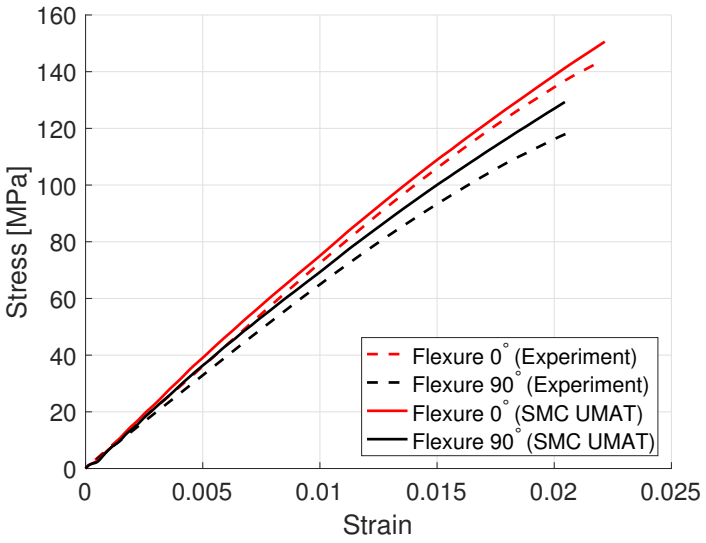

Figure 5.11: Stress-strain response for flexure test

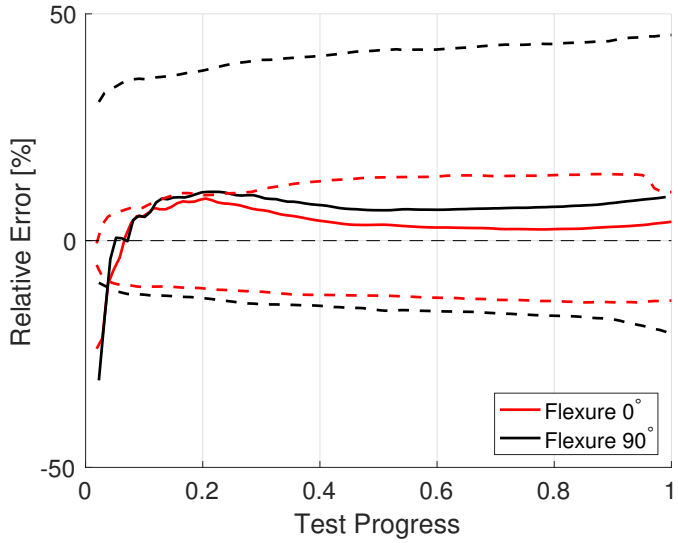

Figure 5.12: Error plot for flexure test prediction vs. experiment

Some examples of possible sources of error includes the non-uniform fibre distribution in the SMC composite or the assumptions made on friction coefficients and material properties in the out-of-plane direction.

5.5 Mesh Convergence Study

A mesh convergence study for each test is conducted to ensure that the stress-strain behaviour predicted has converged for the mesh used in the finite element simulations. Each mesh's element size, measured by the number of elements through the thickness, is successively halved, while attempting to maintain an aspect ratio of 1. It is then verified that the change in work done per unit volume between simulations is less than 5%, indicating that the stress-strain response has converged successfully. The results of the convergence study for the tensile, compressive, in-plane shear and flexure test are shown in Figures 5.13 to 5.16

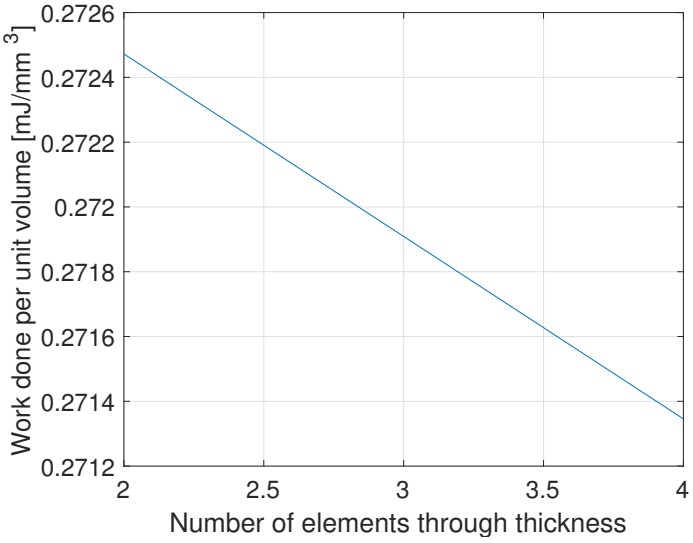

Figure 5.13: Work done vs. number of element across thickness for tensile test

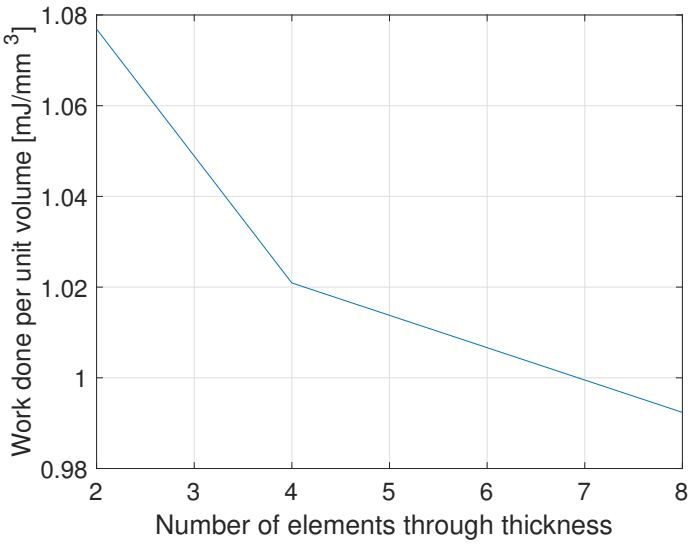

Figure 5.14: Work done vs. number of element across thickness for compressive test

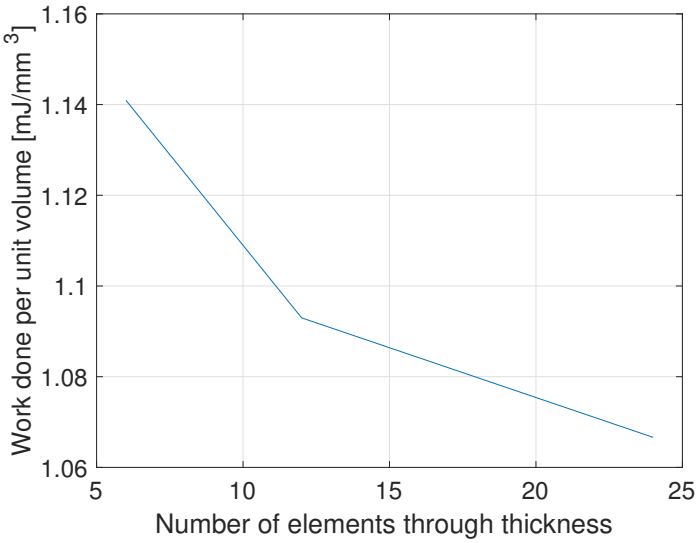

Figure 5.15: Work done vs. number of element across thickness for in-plane shear test

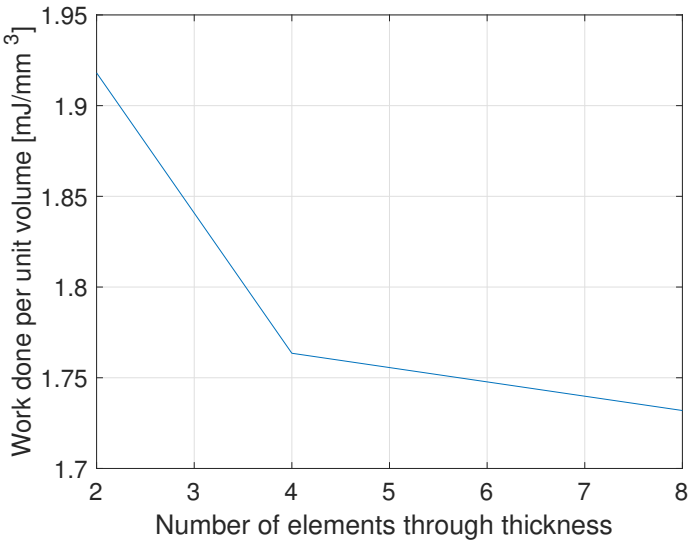

Figure 5.16: Work done vs. number of element across thickness for flexure test

Chapter 6

Parametric Studies

In order to determine the effect of various modeling and material parameters on the flexure simulation results, several parametric studies are conducted on the through-thickness variation in material properties, the presence of tension-compression asymmetry, the friction coefficient between the specimen and fixture and the out-of-plane elastic properties.

6.1 Through-Thickness Variation of Material Properties

One source of error in the flexure simulations would be the local variation in material properties if the fibre volume fraction distribution or orientation distribution in the SMC material is not uniform. For example, there could be a variation in volume fraction across the thickness of the specimen. A variation in volume fraction would result in a variation in various material parameters, such as the elastic moduli and hardening coefficients.

A parametric study is conducted in order to study the effects of the through-thickness variation in properties. Although the variation in local material parameters cannot be identified from the macroscopic experimental testing performed, various distributions are used to quantify the effect of the variation in material properties on the flexure response. The average of each material property across the thickness is kept constant, to ensure that the effect of the through-thickness property variations on the results of the axial and shear load cases would be insignificant.

The first type of distribution is a symmetric distribution, where the material properties towards the mid-plane of the specimen are greater than the material properties towards

the outer surfaces of the specimen. The material parameters are scaled by a factor, SF, where z is the distance from the mid-plane of the specimen. The scaling factor is defined by the function in equation 6.1. This function is formulated to give an average value of 1. A controls the severity of the variation in properties, while B is the offset value used to control the average value.

$$SF = A \cdot |z| + B \tag{6.1}$$

Another distribution studied is asymmetrical, where the material properties vary linearly from the one surface to the other. This could possibly occur due to the effects of gravity during the moulding process. The scaling factor for this distribution is defined by the function in equation 6.2.

$$SF = A \cdot z + B \tag{6.2}$$

This study is performed for the flexure test, in the 0° directions, with each of the eight layers of elements through the thickness assigned material parameters based on the distributions shown in Figure 6.1.

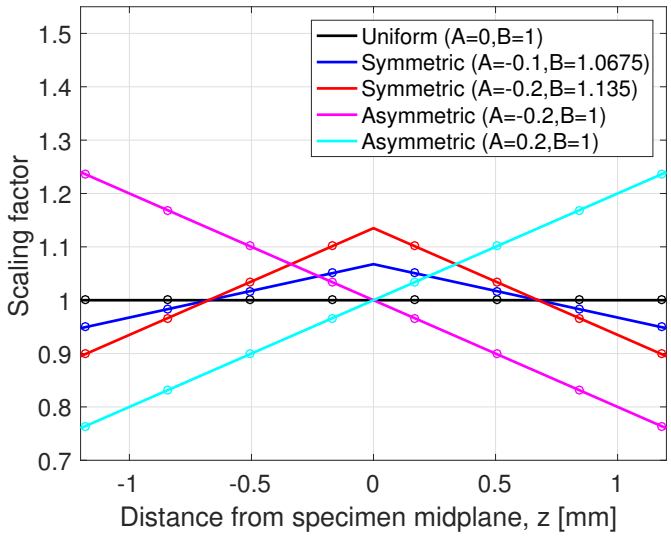

Figure 6.1: Scale factor for elastic and hardening parameters for symmetric and asymmetric distributions

Figures 6.2 and 6.3 show the effect of the variation in through-thickness properties on the flexure response in the 0° direction for the symmetric and asymmetric distributions respectively.

In the study of symmetric distributions, the more severe the through-thickness distribution, indicated by a higher A value, the less stiff the predicted flexure stress-strain response. The decrease in material properties in the outer planes of the specimen had a greater effect than the increase in the material properties in the core of the specimen, resulting in an overall decrease in stiffness in the flexure stress-strain response.

In the study of asymmetric distributions, supporting the specimen on the less stiff side of the specimen results, represented by a positive A value, in a less stiff flexure stress-strain response. This shows that the out-of-plane orientation of specimen can have a significant effect on the result of the experiment if the fibre distribution is not uniform and should be taken into account during the testing process.

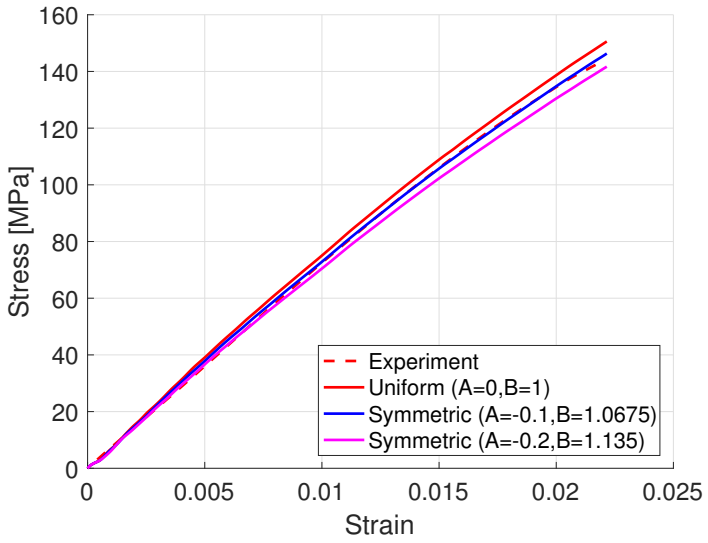

Figure 6.2: Effect of symmetric through-thickness variation in volume fraction on flexure in 0° direction

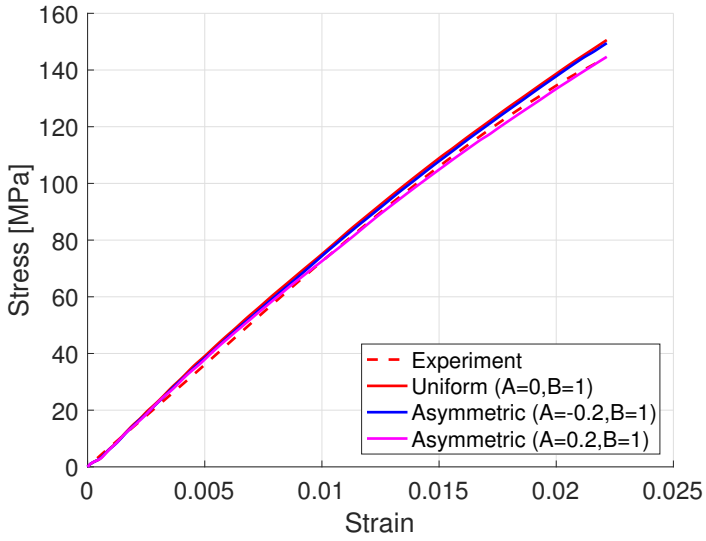

Figure 6.3: Effect of asymmetric through-thickness variation in material properties on flexure in 0° direction

6.2 Tension-Compression Asymmetry

In order to demonstrate the importance of capturing the tension-compression asymmetry of the material when modeling the three-point flexure test, a study is conducted, where the tension-compression asymmetry is removed. The material is assigned properties in the orthotropic axes calibrated using either the tensile test or compressive test. The results of this study in the 0° and 90° flexure tests are shown in Figures 6.4 and 6.5 respectively. From both figures, it is clear that the tension-compression asymmetry has a very significant effect on the flexure response of the material and should definitely be considered when attempting to model such a material.

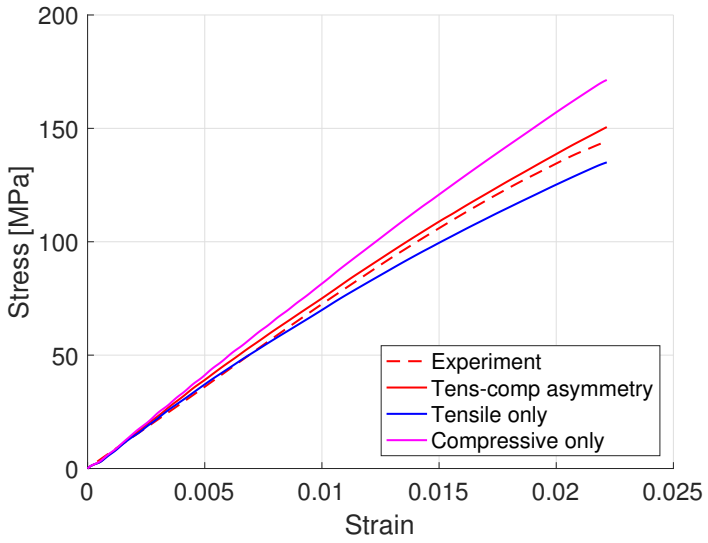

Figure 6.4: Effect of tension-compression asymmetry on flexure in the 0° direction

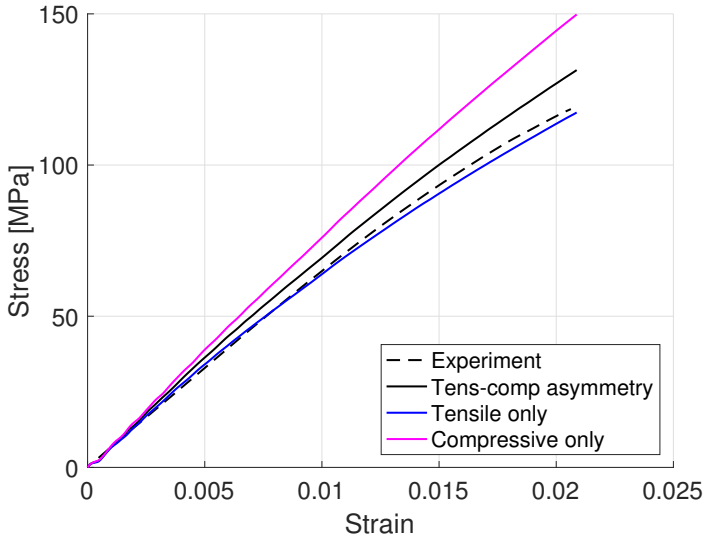

Figure 6.5: Effect of tension-compression asymmetry on flexure in the 90° direction

6.3 Coefficient of Friction

Another simulation parameter which may have had an impact on the flexure test predictions is the coefficient of friction between the testing fixture and the specimen, at the loading fixture and the support fixture. In order to determine the sensitivity of the flexure stress-strain response predicted to the coefficient of friction at these points, a parametric study varying the coefficient of friction between 0.1 and 0.5, at intervals of 0.2, is performed. The study is performed for the flexure test in the 0° direction.

The resulting flexure stress-strain responses from this study are plotted on the same axes in Figure 6.6. It is observed that the lower the coefficient of friction, the less stiff the flexure response. This shows that the coefficient of friction between the specimen and test fixture, which is not available from literature, could indeed be a source of error in the prediction of flexure response.

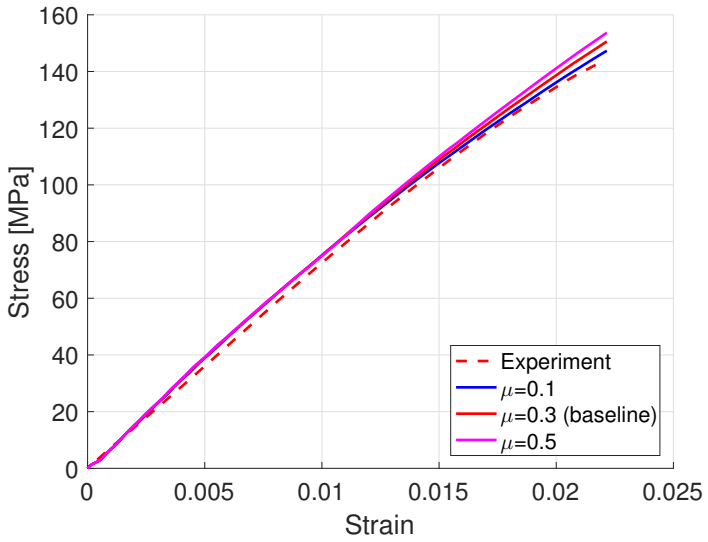

Figure 6.6: Effect of coefficient of friction between specimen and test fixture on flexure in the 0° direction

6.4 Transverse Shear Properties

During the calibration process described in Chapter 5, the transverse shear properties in elasticity are assumed to be equal to the in-plane shear properties. In order to study the validity and effect of this assumption, a parametric study is conducted on the transverse shear moduli, G_{23} and G_{31}, to study their effect on the prediction of flexure stress strain response. The study is performed for the flexure test in the 0° direction. The study is performed with the baseline transverse shear moduli, halved and doubled. The results of this parametric study are shown in Figure 6.7. By comparing the results of the study, it can be concluded that the transverse shear moduli have a negligible effect on the flexure response of the material.

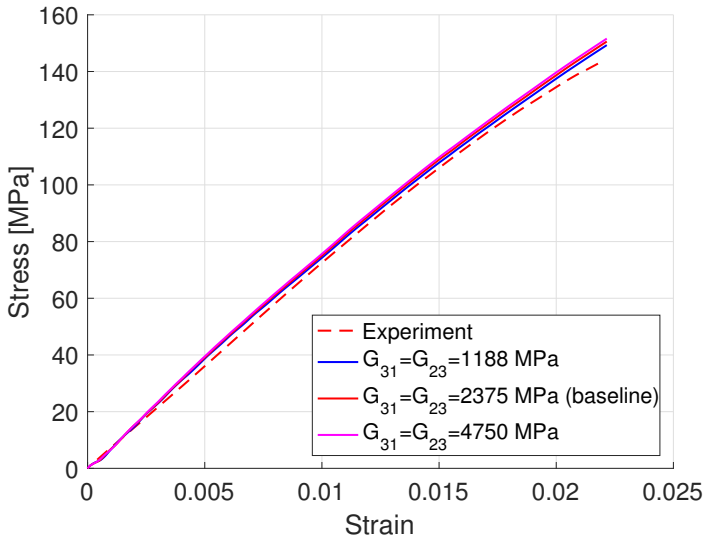

Figure 6.7: Effect of transverse shear elastic moduli on flexure in the 0° direction

6.5 Out-of-Plane Normal Elastic Modulus

During the calibration process described in Chapter 5, it is assumed that $E_3 = E_2$. A parametric study with the out-of-plane normal elastic modulus halved and doubled is conducted for the flexure test in the 0° direction. The results are compared in Figure 6.8. The results of the study show that changing the out-of-plane normal elastic modulus, E_3, has a negligible effect on the flexure response, and therefore the assumptions made are valid.

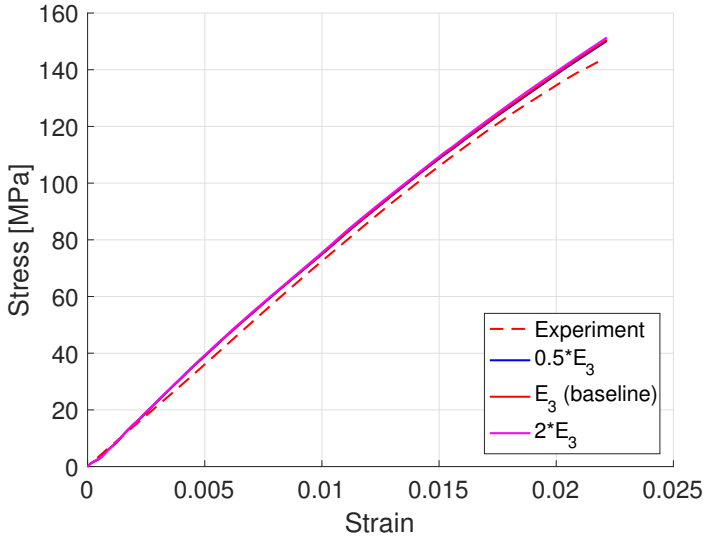

Figure 6.8: Effect of out-of-plane normal elastic modulus on flexure in the 0° direction

Chapter 7

Conclusion

A SMC material was studied experimentally in tension, compression, in-plane shear and three-point bending. It was found through experimental testing that the material demonstrates tension-compression asymmetry and in-plane anisotropy in both the elastic and plastic regime.

Using a macroscopic phenomenological approach, an orthotropic elasto-plastic material model, capable of capturing tension-compression asymmetry, is implemented to capture the experimentally observed behaviour. The model uses a orthotropic elastic constitutive model with a orthotropic yield function, which is also capable of capturing tension-compression asymmetry, and a power law hardening rule.

The material model is implemented as a LS-DYNA user-defined material model to perform lab-scale component level simulations. The material model is calibrated for tensile and compressive tests in the 0° and 90° directions, and the in-plane shear test. The material model is able to capture the behaviour observed in those tests. The calibrated material model was then used to perform simulations of a three-point flexure test. The model is able to predict the flexure stress-strain response of the material within 8% mean absolute error. The predicted flexure stress-strain response of the model is within the variation of experimental data, but overpredicts the average experimental measured stress-strain response. The difference between the predicted and experimental stress-strain curve is likely due to local variations in the material not included in the model.

A parametric study was conducted on various modeling parameters and material parameters, including the through-thickness variation in material properties due to factors, such as volume fraction variation, the out-of-plane elastic moduli, the coefficient of friction

in the test fixture and the presence of tension-compression asymmetry, to determine their effect on the flexure simulation results.

In conclusion, this work has shown that the orthotropic elasto-plastic material model with tension-compression asymmetry, which has been implemented in LS-DYNA as a user-defined material model, is successful in simulating the behaviour of a SMC material in tension, compression, in-plane shear and three-point bending in a component level finite element model. In addition, the importance of capturing the tension-compression asymmetry, and local variations in material properties has been shown through parametric studies.

Chapter 8

Recommendations

The model has been shown to be able to accurately reproduce the experimental behaviour in tension, compression and in-plane shear and is able to predict the flexure response in a three-point bend test. It is able to capture the in-plane anisotropy and tension-compression asymmetry of the material.

In order to improve the accuracy of the model even further, modifications can be made to the material model to be able incorporate the effects of local fibre volume fraction and orientation. Although the model was able to capture the average experimental response, it is observed that there is a large spread in experimental results, likely due to the variation in fibre orientation due to the manufacturing process. By determining the correlation between orientation, fibre volume fraction and the composite material properties, the material behaviour can be better predicted. This is especially important for a larger component where the fibre orientation and volume fraction can vary significantly within the part.

The current material model is also unable to capture the ultimate fracture or failure initiation of the composite. It is able to capture the non-linearity in monotonic loading due to microcracking and plastic deformation using phenomenological plasticity, but macroscopic fracture is not captured. This is important for simulating components in a crash testing scenario where the geometry and failure of the component can determine the way each section of the component contacts and interacts with one another. This can be captured using a failure criterion, such as a maximum strain or stress criteria. Elements in the mesh can be deleted or have their stiffness reduced to represent the failure of the material.

Finally, the material model can be applied to a vehicle component simulation. Depending on the size of the model and its complexity, it may be advantageous to implement the model as a shell element model. This would reduce the amount of simulation time

and model setup time required. Vehicle components also experience loading scenarios with significantly higher strain rates. Therefore, the implementation of a strain rate sensitive hardening model and additional high strain rate testing is highly recommended. Due to the more complex geometry of an actual vehicle component compared to the SMC specimen studied in this work, the fibre structure can be very different and significantly between locations within the component. It is recommended that the proposed model be validated for specimens with various fibre volume fractions and fibre orientation distributions.

References

[1] *ASTM D3039/D3039M-17. Standard Test Method for Tensile Properties of Polymer Matrix Composite Materials*. ASTM International, 2017.

[2] *D6641/D6641M-16e1. Standard Test Method for Compressive Properties of Polymer Matrix Composite Materials Using a Combined Loading Compression (CLC) Test Fixture*. ASTM International, 2016.

[3] *D5379/D5379M-12. Standard Test Method for Shear Properties of Composite Materials by the V-Notched Beam Method*. ASTM International, 2012.

[4] *Plastics: Determination of flexural properties (ISO/DIS 178:2017)*. ISO, 2017.

[5] NHTSA. *National Highway Traffic Safety Administration Strategic Plan 2016-2020*. 2016.

[6] A. Casadei and R. Broda. Impact of vehicle weight reduction on fuel economy for various vehicle architectures. *The Aluminum Association, Inc*, 2007.

[7] W.J. Joost. Reducing vehicle weight and improving U.S. energy efficiency using integrated computational materials engineering. *JOM*, 64(9):1032–1038, Sep 2012.

[8] E.R.H. Fuchs, F.R. Field, R. Roth, and R.E. Kirchain. Strategic materials selection in the automobile body: Economic opportunities for polymer composite design. *Composites Science and Technology*, 68(9):1989 – 2002, 2008.

[9] P. Beardmore and C.F. Johnson. The potential for composites in structural automotive applications. *Composites Science and Technology*, 26(4):251 – 281, 1986.

[10] N. Shama Rao, T.G.A. Simha, K.P. Rao, and G.V.V. Ravi Kumar. *Carbon Composites are Becoming Competitive and Cost Effective*. Infosys Limited, 2017.

[11] F.C. Campbell Jr. *Manufacturing processes for advanced composites*. Elsevier, 2003.

[12] K. Lu. The future of metals. *Science*, 328(5976):319–320, 2010.

[13] J. Stegmann and E. Lund. Discrete material optimization of general composite shell structures. *International Journal for Numerical Methods in Engineering*, 62(14):2009–2027.

[14] H. Fukunaga and G.N. Vanderplaats. Strength optimization of laminated composites with respect to layer thickness and/or layer orientation angle. *Computers & Structures*, 40(6):1429 – 1439, 1991.

[15] E. Mangino, J. Carruthers, and G. Pitarresi. The future use of structural composite materials in the automotive industry. *International Journal of vehicle design*, 44(3-4):211–232, 2007.

[16] R.M. Jones. *Mechanics of composite materials*. CRC press, 2014.

[17] W.D. Callister and D.G. Rethwisch. *Materials Science and Engineering: An Introduction*. Wiley, 2013.

[18] S. Das. The cost of automotive polymer composites: a review and assessment of DOE's lightweight materials composites research. Technical report, Oak Ridge National Lab., TN (US), 2001.

[19] F. Folgar and C.L. Tucker III. Orientation behavior of fibers in concentrated suspensions. *Journal of Reinforced Plastics and Composites*, 3(2):98–119, 1984.

[20] W.C. Jackson, S.G. Advani, and C.L. Tucker. Predicting the orientation of short fibers in thin compression moldings. *Journal of Composite Materials*, 20(6):539–557, 1986.

[21] N. Feld, C. Maeyens, B. Delattre, and N. Grandmaison. Modelling the effect of process-induced anisotropy on the constitutive behavior of chopped fiber composites. *Composites Part A: Applied Science and Manufacturing*, 101:334 – 343, 2017.

[22] K. Potter. *Resin transfer moulding*. Springer Science & Business Media, 2012.

[23] M.G. Bader. Selection of composite materials and manufacturing routes for cost-effective performance. *Composites Part A: Applied Science and Manufacturing*, 33(7):913 – 934, 2002.

[24] M. Oldenbo, D. Mattsson, J. Varna, and L.A. Berglund. Global stiffness of a SMC panel considering process induced fiber orientation. *Journal of Reinforced Plastics and Composites*, 23(1):37–49, 2004.

[25] G.H.B. Donato and M. Bianchi. Pressure dependent yield criteria applied for improving design practices and integrity assessments against yielding of engineering polymers. *Journal of Materials Research and Technology*, 1(1):2 – 7, 2012.

[26] A.M. Hartl, M. Jerabek, and R.W. Lang. Anisotropy and compression/tension asymmetry of PP containing soft and hard particles and short glass fibers. *Express Polymer Letters*, 9(7):658–670, 2015.

[27] A.M. Hartl, M. Jerabek, P. Freudenthaler, and R.W. Lang. Orientation-dependent compression/tension asymmetry of short glass fiber reinforced polypropylene: Deformation, damage and failure. *Composites Part A: Applied Science and Manufacturing*, 79:14 – 22, 2015.

[28] J.D. Littell, C.R. Ruggeri, R.K. Goldberg, G.D. Roberts, W.A. Arnold, and W.K. Binienda. Measurement of epoxy resin tension, compression, and shear stress-strain curves over a wide range of strain rates using small test specimens. *Journal of Aerospace Engineering*, 21(3):162–173, 2008.

[29] W. Chen, F. Lu, and M. Cheng. Tension and compression tests of two polymers under quasi-static and dynamic loading. *Polymer Testing*, 21(2):113 – 121, 2002.

[30] J. Rösler, H. Harders, and M. Baeker. *Mechanical behaviour of engineering materials: metals, ceramics, polymers, and composites*. Springer Science & Business Media, 2007.

[31] R. Elleuch and Wafa Taktak. Viscoelastic behavior of HDPE polymer using tensile and compressive loading. *Journal of Materials Engineering and Performance*, 15(1):111–116, Feb 2006.

[32] C.T. Sun and R.S. Vaidya. Prediction of composite properties from a representative volume element. *Composites Science and Technology*, 56(2):171 – 179, 1996.

[33] J. Aboudi. Micromechanical analysis of composites by the method of cells. *Applied Mechanics Reviews*, 42(7):193–221, 1989.

[34] S.Y. Hsu, T.J. Vogler, and S. Kyriakides. Inelastic behavior of an AS4/PEEK composite under combined transverse compressionand shear.Part II: modeling. *International Journal of Plasticity*, 15(8):807 – 836, 1999.

[35] G. Lielens, P. Pirotte, A. Couniot, F. Dupret, and R. Keunings. Prediction of thermo-mechanical properties for compression moulded composites. *Composites Part A: Applied Science and Manufacturing*, 29(1):63 – 70, 1998.

[36] T. Mori and K. Tanaka. Average stress in matrix and average elastic energy of materials with misfitting inclusions. *Acta metallurgica*, 21(5):571–574, 1973.

[37] I. Doghri and L. Tinel. Micromechanics of inelastic composites with misaligned inclusions: Numerical treatment of orientation. *Computer Methods in Applied Mechanics and Engineering*, 195(13):1387 – 1406, 2006.

[38] D.J. O'Dwyer, N.P. O'Dowd, and C.T. McCarthy. Micromechanical investigation of damage processes at composite-adhesive interfaces. *Composites Science and Technology*, 86:61 – 69, 2013.

[39] V.I. Kushch, S.V. Shmegera, and L. Mishnaevsky. Explicit modeling the progressive interface damage in fibrous composite: Analytical vs. numerical approach. *Composites Science and Technology*, 71(7):989 – 997, 2011.

[40] G.M. Odegard, T.C. Clancy, and T.S. Gates. Modeling of the mechanical properties of nanoparticle/polymer composites. *Polymer*, 46(2):553 – 562, 2005.

[41] F.T. Fisher and L.C. Brinson. Viscoelastic interphases in polymermatrix composites: theoretical models and finite-element analysis. *Composites Science and Technology*, 61(5):731 – 748, 2001.

[42] S. Nie and C. Basaran. A micromechanical model for effective elastic properties of particulate composites with imperfect interfacial bonds. *International Journal of Solids and Structures*, 42(14):4179 – 4191, 2005.

[43] Y. Benveniste, G.J. Dvorak, and T. Chen. Stress fields in composites with coated inclusions. *Mechanics of Materials*, 7(4):305 – 317, 1989.

[44] T. Sabiston, M. Mohammadi, M. Cherkaoui, J. Lévesque, and K. Inal. Micromechanics for a long fibre reinforced composite model with a functionally graded interphase. *Composites Part B: Engineering*, 84:188 – 199, 2016.

[45] T. Sabiston, M. Mohammadi, M. Cherkaoui, J. Lévesque, and K. Inal. Micromechanics based elasto-visco-plastic response of long fibre composites using functionally graded interphases at quasi-static and moderate strain rates. *Composites Part B: Engineering*, 100:31 – 43, 2016.

[46] G.P. Carman and K.L. Reifsnider. Micromechanics of short-fiber composites. *Composites Science and Technology*, 43(2):137 – 146, 1992.

[47] J. Aboudi, S.M. Arnold, and B.A. Bednarcyk. *Micromechanics of composite materials: a generalized multiscale analysis approach*. Butterworth-Heinemann, 2012.

[48] G. Panasenko. *Multi-scale Modelling for Structures and Composites*. Springer Netherlands, Dordrecht, 2005.

[49] M.M. Mehrabadi and S.C. Cowin. Eigentensors of linear anisotropic elastic materials. *The Quarterly Journal of Mechanics and Applied Mathematics*, 43(1):15–41, 1990.

[50] B.M. Lempriere. Poisson's ratio in orthotropic materials. *AIAA Journal*, 6(11):2226–2227, 1968.

[51] F. Bron and J. Besson. A yield function for anisotropic materials application to aluminum alloys. *International Journal of Plasticity*, 20(4-5):937–963, 2004.

[52] R. von Mises. Mechanik der festen körper im plastisch-deformablen zustand. *Nachrichten von der Gesellschaft der Wissenschaften zu Göttingen, Mathematisch-Physikalische Klasse*, 1913(4):582–592, 1913.

[53] W.F. Hosford. A generalized isotropic yield criterion. *Journal of Applied Mechanics*, 39(2):607–609, 1972.

[54] R. Hill. A theory of the yielding and plastic flow of anisotropic metals. *Proc. R. Soc. Lond. A*, 193(1033):281–297, 1948.

[55] C. Kohar. *Multi-scale Modeling and Optimization of Energy Absorption and Anisotropy in Aluminum Alloys*. PhD thesis, 2017.

[56] F. Barlat and K. Lian. Plastic behavior and stretchability of sheet metals. part i: A yield function for orthotropic sheets under plane stress conditions. *International Journal of Plasticity*, 5(1):51 – 66, 1989.

[57] F. Barlat, D.J. Lege, and J.C. Brem. A six-component yield function for anisotropic materials. *International Journal of Plasticity*, 7(7):693 – 712, 1991.

[58] F. Barlat, J.C. Brem, J.W. Yoon, K. Chung, R.E. Dick, D.J. Lege, F. Pourboghrat, S.-H. Choi, and E. Chu. Plane stress yield function for aluminum alloy sheets-part 1: theory. *International Journal of Plasticity*, 19(9):1297 – 1319, 2003.

[59] J.N. Sultan and F.J. McGarry. Effect of rubber particle size on deformation mechanisms in glassy epoxy. *Polymer Engineering & Science*, 13(1):29–34, 1973.

[60] O. Cazacu, B. Plunkett, and F. Barlat. Orthotropic yield criterion for hexagonal closed packed metals. *International Journal of Plasticity*, 22(7):1171 – 1194, 2006.

[61] J.O. Hallquist. *LS-DYNA Theory Manual*. Livermore Software Technology Corporation, 2006.

[62] P. Ludwik. *Elemente der Technologischen Mechanik*. Springer-Verlag Berlin Heidelberg, 1909.

[63] G.R. Johnson and W.H. Cook. Fracture characteristics of three metals subjected to various strains, strain rates, temperatures and pressures. *Engineering fracture mechanics*, 21(1):31–48, 1985.

[64] LSTC. *LS-DYNA Keyword User's Manual, Volume II, Material Models*. Livermore Software Technology Corporation, 2012.

[65] F.K. Chang and K.Y. Chang. Post-failure analysis of bolted composite joints in tension or shear-out mode failure. *Journal of Composite Materials*, 21(9):809–833, 1987.

[66] A. Matzenmiller, J. Lubliner, and R.L. Taylor. A constitutive model for anisotropic damage in fiber-composites. *Mechanics of Materials*, 20(2):125 – 152, 1995.

[67] X. Xiao, M.E. Botkin, and N.L. Johnson. Axial crush simulation of braided carbon tubes using MAT58 in LS-DYNA. *Thin-Walled Structures*, 47(6):740 – 749, 2009.

[68] K. Schweizerhof, K. Weimar, T. Munz, and T. Rottner. Crashworthiness analysis with enhanced composite material models in LS-DYNA - merits and limits. In *LS-DYNA World Conference, Detroit, MI*, pages 1–17, 1998.

[69] J. Huang and X. Wang. Numerical and experimental investigations on the axial crushing response of composite tubes. *Composite Structures*, 91(2):222 – 228, 2009.

[70] H. El-Hage, P.K. Mallick, and N. Zamani. Numerical modelling of quasi-static axial crush of square aluminium-composite hybrid tubes. *International Journal of Crashworthiness*, 9(6):653–664, 2004.

[71] A.G. Mamalis, D.E. Manolakos, M.B. Ioannidis, and D.P. Papapostolou. The static and dynamic axial collapse of CFRP square tubes: Finite element modelling. *Composite Structures*, 74(2):213 – 225, 2006.

[72] Euro NCAP. Assessment protocol - pedestrian protection. 2018.

[73] ANCAP. ANCAP test protocol. Pedestrian protection v8.3. 2017.

[74] G. Oldenbo, A. van den Berg, R.W.G. Anderson, and B. Linke. The pedestrian protection in vehicle impacts: Desmystifying pedestrian testing procedures and assessment. *Australasian College of Road Safety Conference*, 2013.

[75] T.L. Teng and V.L. Ngo. Analyzing pedestrian head injury to design pedestrian-friendly hoods. *International Journal of Automotive Technology*, 12(2):213–224, Apr 2011.

[76] C.K. Ramesh, S. Srikari, and M.L.J. Suman. Design of hood stiffener of a sedan car for pedestrian safety. *SASTech, Journal*, 11(2):67–73, 2012.

[77] A. Masoumi, M.H. Shojaeefard, and A. Najibi. Comparison of steel, aluminum and composite bonnet in terms of pedestrian head impact. *Safety Science*, 49(10):1371 – 1380, 2011.

[78] G. Belingardi and G. Vadori. Low velocity impact tests of laminate glass-fiber-epoxy matrix composite material plates. *International Journal of Impact Engineering*, 27(2):213 – 229, 2002.

[79] C.K.L. Davies, S. Turner, and K.H. Williamson. Flexed plate impact testing of carbon fibre-reinforced polymer composites. *Composites*, 16(4):279 – 285, 1985.

[80] J.D. Winkel and D.F. Adams. Instrumented drop weight impact testing of cross-ply and fabric composites. *Composites*, 16(4):268 – 278, 1985.

[81] S. Heimbs, S. Heller, P. Middendorf, F. Hähnel, and J. Weiße. Low velocity impact on CFRP plates with compressive preload: Test and modelling. *International Journal of Impact Engineering*, 36(10):1182 – 1193, 2009.

[82] F. Caputo, A. De Luca, G. Lamanna, R. Borrelli, and U. Mercurio. Numerical study for the structural analysis of composite laminates subjected to low velocity impact. *Composites Part B: Engineering*, 67:296 – 302, 2014.

[83] M.A. Perez, L. Gil, and S. Oller. Non-destructive testing evaluation of low velocity impact damage in carbon fiber-reinforced laminated composites. *Ultragarsas" Ultrasound"*, 66(2):21–27, 2011.

[84] *ASTM D7136/D7136M-15 Standard Test Method for Measuring the Damage Resistance of a Fiber-Reinforced Polymer Matrix Composite to a Drop-Weight Impact Event*. ASTM International, 2015.

[85] T. Munikenche Gowda, A.C.B. Naidu, and R. Chhaya. Some mechanical properties of untreated jute fabric-reinforced polyester composites. *Composites Part A: Applied Science and Manufacturing*, 30(3):277 – 284, 1999.

[86] C.M. Manjunatha, A.C. Taylor, A.J. Kinloch, and S. Sprenger. The tensile fatigue behaviour of a silica nanoparticle-modified glass fibre reinforced epoxy composite. *Composites Science and Technology*, 70(1):193 – 199, 2010.

[87] M. Jawaid, H.P.S. Abdul Khalil, A. Abu Bakar, and P. Noorunnisa Khanam. Chemical resistance, void content and tensile properties of oil palm/jute fibre reinforced polymer hybrid composites. *Materials & Design*, 32(2):1014 – 1019, 2011.

[88] J. Montesano, Z. Fawaz, and H. Bougherara. Non-destructive assessment of the fatigue strength and damage progression of satin woven fiber reinforced polymer matrix composites. *Composites Part B: Engineering*, 71:122 – 130, 2015.

[89] J. Montesano, Z. Fawaz, K. Behdinan, and C. Poon. Fatigue damage characterization and modeling of a triaxially braided polymer matrix composite at elevated temperatures. *Composite Structures*, 101:129 – 137, 2013.

[90] D.R. Bortz, C. Merino, and I. Martin-Gullon. Mechanical characterization of hierarchical carbon fiber/nanofiber composite laminates. *Composites Part A: Applied Science and Manufacturing*, 42(11):1584 – 1591, 2011.

[91] K. Sabeel Ahmed and S. Vijayarangan. Tensile, flexural and interlaminar shear properties of woven jute and jute-glass fabric reinforced polyester composites. *Journal of Materials Processing Technology*, 207(1):330 – 335, 2008.

[92] J. Zhang, K. Chaisombat, S. He, and C.H. Wang. Hybrid composite laminates reinforced with glass/carbon woven fabrics for lightweight load bearing structures. *Materials & Design (1980-2015)*, 36:75 – 80, 2012. Sustainable Materials, Design and Applications.

[93] N.R. Adsit. Compression testing of graphite/epoxy. In *Compression Testing of Homogeneous Materials and Composites*. ASTM International, 1983.

[94] *D3410/D3410M-16. Standard test method for compressive properties of polymer matrix composite materials with unsupported gage section by shear loading*. ASTM International, 2016.

[95] *D695-15. Standard test method for compressive properties of rigid plastics*. ASTM International, 2015.

[96] D.F. Adams. Tabbed versus untabbed fiber-reinforced composite compression specimens. In *Composite Materials: Testing, Design, and Acceptance Criteria*. ASTM International, 2002.

[97] A. Jumahat, C. Soutis, F.R. Jones, and A. Hodzic. Fracture mechanisms and failure analysis of carbon fibre/toughened epoxy composites subjected to compressive loading. *Composite Structures*, 92(2):295 – 305, 2010.

[98] S. Lee and M. Munro. Evaluation of in-plane shear test methods for advanced composite materials by the decision analysis technique. *Composites*, 17(1):13–22, 1986.

[99] D.E. Walrath and D.F. Adams. The losipescu shear test as applied to composite materials. *Experimental mechanics*, 23(1):105–110, 1983.

[100] D.F. Adams and D.E. Walrath. Iosipescu shear properties of smc composite materials. In *Composite Materials: Testing and Design (6th Conference)*. ASTM International, 1982.

[101] B.F. Yousif, A. Shalwan, C.W. Chin, and K.C. Ming. Flexural properties of treated and untreated kenaf/epoxy composites. *Materials & Design*, 40:378 – 385, 2012.

[102] P.O. Hagstrand, F. Bonjour, and J.A.E. Mnson. The influence of void content on the structural flexural performance of unidirectional glass fibre reinforced polypropylene composites. *Composites Part A: Applied Science and Manufacturing*, 36(5):705 – 714, 2005.

[103] A.K. Bledzki, A. Jaszkiewicz, and D. Scherzer. Mechanical properties of PLA composites with man-made cellulose and abaca fibres. *Composites Part A: Applied Science and Manufacturing*, 40(4):404 – 412, 2009.

[104] O.M.L. Asumani, R.G. Reid, and R. Paskaramoorthy. The effects of alkalisilane treatment on the tensile and flexural properties of short fibre non-woven kenaf reinforced polypropylene composites. *Composites Part A: Applied Science and Manufacturing*, 43(9):1431 – 1440, 2012.

[105] *D790-15. Standard Test Methods for Flexural Properties of Unreinforced and Reinforced Plastics and Electrical Insulating Materials*. ASTM International, 2015.

[106] B.W. Williams, C.H.M. Simha, N. Abedrabbo, R. Mayer, and M.J. Worswick. Effect of anisotropy, kinematic hardening, and strain-rate sensitivity on the predicted axial crush response of hydroformed aluminium alloy tubes. *International Journal of Impact Engineering*, 37(6):652 – 661, 2010. Impact Loading of Lightweight Structures.

[107] C.P. Kohar, M. Mohammadi, R.K. Mishra, and K. Inal. The effects of the yield surface curvature and anisotropy constants on the axial crush response of circular crush tubes. *Thin-Walled Structures*, 106:28 – 50, 2016.

[108] J.W. Yoon, F. Barlat, R.E. Dick, K. Chung, and T.J. Kang. Plane stress yield function for aluminum alloy sheetspart II: FE formulation and its implementation. *International Journal of Plasticity*, 20(3):495 – 522, 2004. Owen Richmond Memorial Special Issue.

[109] N. Abedrabbo, F. Pourboghrat, and J. Carsley. Forming of AA5182-O and AA5754-O at elevated temperatures using coupled thermo-mechanical finite element models. *International Journal of Plasticity*, 23(5):841 – 875, 2007.

[110] K. Levenberg. A method for the solution of certain non-linear problems in least squares. *Quarterly of applied mathematics*, 2(2):164–168, 1944.

[111] D.W. Marquardt. An algorithm for least-squares estimation of nonlinear parameters. *Journal of the society for Industrial and Applied Mathematics*, 11(2):431–441, 1963.

[112] C.J. Willmott and K. Matsuura. Advantages of the mean absolute error (MAE) over the root mean square error (RMSE) in assessing average model performance. *Climate Research*, 30(1):79–82, 2005.